

**Electrochemical, Spectroscopic and Acid-base Properties of
Pyridylporphyrins in Nonaqueous Media**

A Thesis Presented to
the Faculty of the Department of Chemistry
University of Houston

In Partial Fulfillment
of the Requirements for the Degree
Master of Science

By
Jialiang Zhu

August 2016

**Electrochemical, Spectroscopic and Acid-base Properties of
Pyridylporphyrins in Nonaqueous Media**

Jialiang Zhu

APPROVED:

Dr. Karl M. Kadish, Chairman

Dr. John L. Bear

Dr. Steven Baldelli

Dr. Thomas S. Teets

Dr. Eric Van Caemelbecke

Dean, College of Natural Sciences and Mathematics

Dedication

This thesis is dedicated to

My parents, Yang Zhu and Shizhen Cao, my sister, Ke Cao

and

my loved Lu Chen

Acknowledgements

I would like to express my sincere appreciation to my supervisor, Dr. Karl M. Kadish, for his guidance and support throughout my graduate studies.

I would like to express my sincere gratitude to my parents for their support, encouragement and love.

I would like to thank Dr. Roger Guilard, Dr. Claude P. Gros, Dr. Roberto Paolesse, and Dr. Ravindra K. Pandey for their comments and contribution to the projects and for providing the compounds studied in this thesis.

The financial support provided by the Robert A. Welch Foundation is also gratefully acknowledged.

I would finally like to thank my colleagues for working with me all these years.

**ELECTROCHEMICAL, SPECTROSCOPIC AND ACID-BASE
PROPERTIES OF PYRIDYLPORPHYRINS
IN NONAQUEOUS MEDIA**

An Abstract of a Thesis
Presented to
the Faculty of the Department of Chemistry
University of Houston

In Partial Fulfillment
of the Requirements for the Degree
Master of Science

By
Jialiang Zhu
August 2016

Abstract

This thesis describes the electrochemical, spectroscopic and acid-base properties of pyridylporphyrins, tetramethylpyridyl porphyrins and corroles in nonaqueous media. Several corroles are also examined. Free-base and metal derivatives (Co^{II} , Ni^{II} , Cu^{II} and Zn^{II}) of pyridylporphyrins possessing one, two or four pyridyl *meso*-substituents were examined before, during and after the addition of protons to solution in the form of trifluoroacetic acid (TFA). The free-base (metal-free) pyridylporphyrins undergo an initial protonation on the pyridyl substituents and this is followed by protonation of the central nitrogen atoms in a second step. The pyridylporphyrins with metal centers are only protonated at the *meso*-pyridyl groups. Both sites of protonation are associated with specific changes in the electrochemical and spectroscopic properties of the compounds. The utilized solvent was shown to have an effect on the protonation constants, which varied from 10^2 to 10^4 , depending upon the specific compound. The tetrapositively-charged free-base tetra-*N*-methylpyridylporphyrins possess four Cl^- , Br^- , I^- or PhSO_3^- counteranions and the electrochemistry of these compounds was examined in DMF or DMSO, containing 0.1 M tetra-*n*-butylammonium hexafluorophosphate (TBAPF_6) or tetra-*n*-butylammonium iodide (TBAI). These measurements were made in order to study the interaction of the counteranion, the solvent and the supporting electrolyte on the reductions. Finally, the electrochemical properties of iron ferrocenylcorroles with NO , C_6H_5 or Cl^- axial ligands were examined in PhCN containing 0.05 M tetrakis-fluorophenylborate (TFAB).

Table of Contents

Title	Page
List of Abbreviations.....	xi
List of Charts.....	xiii
List of Figures.....	xiv
List of Tables.....	xvi
List of Schemes.....	xvii
Chapter One Introduction.....	1
1.1 Outline of Research in This Thesis.....	2
1.2 Porphyrins.....	2
1.3 Pyridylporphyrins and Tetra-4- <i>N</i> -Methylpyridylporphyrins.....	4
1.4 Corroles.....	6
1.5 Electrochemistry and Spectroelectrochemistry.....	7
1.5.1 UV-Vis Spectroscopic Characterization of Porphyrins.....	7
1.5.2 Electrochemistry.....	7
1.5.3 Spectroelectrochemistry.....	9
1.6 References.....	11
Chapter Two Experimental Methods.....	16

2.1	Cyclic Voltammetry.....	16
2.2	UV-visible Spectroelectrochemistry Methods.....	17
2.3	Spectral Titration Methods for Determination of Equilibrium Constants.....	20
2.4	Other Experimental Methods.....	23
2.4.1	Degassing the Solution.....	23
2.5	Chemicals and Investigated Compounds.....	23
2.5.1	Chemicals.....	23
2.5.2	Investigated Compounds.....	23
2.6	References.....	24
Chapter Three	Electrochemistry and Acid-Base Properties of Free-base Pyridylporphyrins in Nonaqueous Media.....	26
3.1	Introduction.....	27
3.2	Results and Discussion.....	30
3.2.1	Spectroscopic Characterization.....	30
3.2.2	UV-Vis Spectral Monitoring of Protonation	33
3.2.3	Protonated Pyridylporphyrins.....	40
3.3	Conclusions.....	44
3.4	References.....	45

Chapter Four	Electrochemistry and Acid-Base Properties of Metallopyridylporphyrins in Nonaqueous Media.....	46
4.1	Introduction.....	47
4.2	Results and Discussion.....	49
4.2.1	UV-Vis Spectral Monitoring of Metallopyridylporphyrins Protonation	49
4.2.2	Electrochemistry and Spectroelectrochemistry.....	51
4.2.3	Aggregation of Zinc Pyridylporphyrin Before Addition of Acid.....	55
4.2.4	Aggregation of Cobalt Pyridylporphyrin After addition of Acid.....	58
4.3	Conclusions.....	61
4.4	References.....	62
Chapter Five	Electrochemical Studies of Free-base Tetra-N-Methylpyridylporphyrins.....	64
5.1	Introduction.....	65
5.2	Results and Discussion.....	69
5.2.1	Electrochemistry.....	69
5.2.2	UV-Vis Spectroscopy.....	72
5.3	Conclusions.....	75
5.4	References.....	76

Chapter Six	Electrochemical Studies of Iron Ferrocenylcorroles.....	77
6.1	Introduction.....	78
6.2	Results and Discussion.....	80
6.2.1	Electrochemistry in PhCN.....	80
6.3	Conclusions.....	86
6.4	References.....	87

List of Abbreviations

Abbreviation	Meaning
A	absorbance
CE	counter electrode
CH ₂ Cl ₂	dichloromethane
CV	cyclic voltammetry
DMF	N,N'-dimethylformamide
DMSO	dimethylsulfoxide
$\Delta E_{1/2}$	difference in half-wave potential between two processes
$E_{1/2}$	half-wave potential
E_p	peak potential (by cyclic voltammetry)
E_{pa}	anodic peak potential (by cyclic voltammetry)
E_{pc}	cathodic peak potential (by cyclic voltammetry)
ϵ	molar absorptivity
FTIR	fourier transform infrared
HOMO	highest occupied molecular orbital
i_{pa}	anodic peak current (by cyclic voltammetry)
i_{pc}	cathodic peak current (by cyclic voltammetry)
LUMO	lowest unoccupied molecular orbital
λ_{max}	wavelength at a specific peak maximum

OEP	dianion of 2,3,7,8,12,13,17,18-octaethylporphyrin
py	pyridine
PhCN	benzonitrile
RE	reference electrode
SCE	saturated calomel electrode
TBACl	tetra- <i>n</i> -butylammonium chloride
TBABr	tetra- <i>n</i> -butylammonium bromide
TBAI	tetra- <i>n</i> -butylammonium iodide
TBAP	tetra- <i>n</i> -butylammonium perchlorate
TFAB	Tetrakis-fluorophenyl borate
TFA	trifluoroacetic acid
TMPyP	tetra- <i>N</i> -methylpyridylporphyrin
TPP	5,10,15,20-tetraphenylporphyrin dianion
WE	working electrode
H ₂ TPP	5,10,15,20-tetraphenylporphyrin
H ₂ Py ₄ Por	<i>meso</i> -tetra(4-pyridyl)porphyrin
H ₂ Py ₃ Por	<i>meso</i> -tetra(3-pyridyl)porphyrin
H ₂ Py ₂ Por	<i>meso</i> -tetra(2-pyridyl)porphyrin
TPPS	tetraphenylporphinesulfonate
TMPyP4	tetra-(<i>N</i> -methyl-4-pyridyl)porphyrin

List of Charts

Chart		Page
Chart 1-1.	Structure of porphyrin (porphine) and labeling system	4
Chart 1-2.	Structures of (a) a <i>meso</i> -tetrapyridylporphyrin and (b) a positively charged tetra- <i>N</i> -methylpyridylporphyrin (TMPyP) where the X ⁻ counteranions are shown as dissociated	6
Chart 3-1.	Structures of investigated pyridylporphyrins	29
Chart 4-1.	Structures of investigated metallopyridylporphyrins	48
Chart 5-1.	Molecular structures of the investigated porphyrins	68
Chart 6-1.	Molecular structures of investigated Fe corroles	79

List of Figures

Figure		Page
Figure 1-1.	Example of cyclic voltammogram showing an initial reduction and reoxidation on the reverse scan	9
Figure 2-1.	Schematic illustration of the home-built electrochemical cell with the working counter and reference electrodes	18
Figure 2-2.	Cyclic voltammetry waveform showing a scan between 0.8 to -0.2 V ...	19
Figure 2-3.	Schematic illustration of the thin-layer UV-visible spectroelectrochemical cell	21
Figure 2-4.	An example of UV-visible spectra changes during titration, where A_0 is the initial absorbance, A_i is the absorbance at a given point in the titration and A_f is the absorbance in the final step	22
Figure 3-1.	UV-vis spectra of investigated free-base pyridylporphyrins in CH_2Cl_2 and pyridine	31
Figure 3-2.	UV-vis spectral changes during titration of free-base porphyrins 1H₂ and H₂TPP in (a) PhCN and (b) DMF with TFA and analysis of data for calculation of proton addition	35
Figure 3-3.	UV-vis spectral changes during titration of (a) H₂TPP , (b) 1H₂ and (c) 2H₂ with TFA and diagnostic log-log plots for calculation of proton constants	37
Figure 3-4.	Cyclic voltammograms of H₂TPP , H₂Py(PhMe)₃P and H₂Py₂(PhMe)₂P ($\sim 10^{-4}$ M) in (a) DMF containing 0.1 M TBAP, (b) DMF containing 0.1 M TBAP and 5.0 eq TFA and (c) DMF containing excess TFA	42

Figure 4-1.	UV-visible spectral changes of 1Ni , 1Cu and 1Zn in PhCN during titration with TFA. The figure insets show the Hill plots used for analysis	50
Figure 4-2.	Cyclic voltammograms of CuPy(PhMe) ₃ Por (1Cu), NiPy(PhMe) ₃ Por (1Ni) and ZnPy(PhMe) ₃ Por (1Zn) in PhCN containing 0.1 M TBAP.....	52
Figure 4-3.	(a) Cyclic voltammograms and (b) UV-vis spectral changes for oxidation and reduction of CoPy(PhMe) ₃ Por 1Co in pyridine	55
Figure 4-4.	UV-visible spectra changes of 2Zn in PhCN during titration with TFA. The figure inset shows the Hill plot used for analysis	56
Figure 4-5.	Spectral changes of CoPy ₂ (PhMe) ₂ Por 2Co (a) upon a one electron oxidation at 0.30V in pyridine and (b) during the first protonation step of the neutral porphyrin in CH ₂ Cl ₂	59
Figure 5-1.	Cyclic voltammograms of [H ₂ TMPyP] ⁴⁺ (X ⁻) ₄ in DMSO containing 0.1 M (a) TBAPF ₆ and (b) TBAI	70
Figure 5-2.	Cyclic voltammograms of [H ₂ TMPyP] ⁴⁺ (X ⁻) ₄ in DMF containing 0.1 M (a) TBAPF ₆ or (b) TBAI	71
Figure 6-1.	Cyclic voltammograms of TFeCorrFe ^{III} (NO), TFeCorrFe ^{IV} (C ₆ H ₅) and TFeCorrFe ^{IV} (Cl) in PhCN, containing 0.05 M TFAB at a scan rate of 0.1V/s	83
Figure 6-2.	Cyclic voltammograms of TFeCorrFe ^{III} (NO), TFeCorrFe ^{III} (C ₆ H ₅) and TFeCorrFe ^{IV} (Cl) in PhCN, containing 0.1 M TBAP at a scan rate of 0.1 V/s	84

List of Tables

Table		Page
Table 3-1.	UV/vis spectra data λ_{\max} (log ϵ), nm for H ₂ TPP, 1H₂ , 2H₂ and 4H₂ in different solvents.....	32
Table 3-2.	UV-vis spectra data λ_{\max} , nm for H ₄ TPP ²⁺ , 1H₅³⁺ and 2H₆⁴⁺ in DMF	33
Table 3-3.	Protonation constants for mono- and di-pyridyl free-base porphyrins in different solvents	36
Table 4-1.	Half-wave potentials (V vs SCE) of investigated mono- and di-pyridylporphyrins in different solvents containing 0.1 M TBAP. Scan rate = 0.1 V/s	54
Table 5-1.	Half-wave reduction potentials of TMPyPX ₄ in DMSO or DMF containing 0.1M TBAI or 0.1M TBAPF ₆	73
Table 5-2.	UV-vis data of [H ₂ TMPyP] ⁴⁺ (X ⁻) ₄ in DMSO or DMF containing 0.1M TBAI or 0.1M TBAPF ₆	74

List of Schemes

Scheme	Page
Scheme 3-1. Proposed protonation mechanism for free-base pyridylporphyrins	39
Scheme 4-1. Proposed mechanism for oxidation and reduction of $\text{Co}^{\text{II}}\text{Py}(\text{PhMe})_3\text{Por}$ 1Co or $\text{Co}^{\text{II}}\text{Py}_2(\text{PhMe})_2\text{Por}$ 2Co in pyridine, where P represents $\text{Py}(\text{PhMe})_3\text{Por}$ or $\text{Py}_2(\text{PhMe})_2\text{Por}$ and pyrd = pyridine. Only the central metal ion (Co^{III} , Co^{II} or Co^{I}) and axial ligand (pyrd) are shown). The initial 5-coordinate porphyrin in solutions of pyridine is shown in the red box	57
Scheme 4-2. Proposed protonation and aggregation of oxidized $\text{CoPy}_2(\text{PhMe})_2\text{Por}$ 1Co	60
Scheme 6-1. Reduction mechanism of $\text{TFcCorrFe}^{\text{IV}}(\text{Cl})$ in PhCN, containing 0.05 M TFAB	85

Chapter One

Introduction

1.1 Outline of Research in This Thesis

The research in this thesis involves electrochemical, spectroelectrochemical, and spectroscopic studies of four types of compounds:

(i) free-base porphyrins with different numbers of pyridyl substituents at the *meso*-positions of the macrocycle,

(ii) metalloporphyrins with different numbers of pyridyl substituents at the macrocycle *meso*-positions and different metal centers,

(iii) free-base tetra-*N*-methylpyridylporphyrins,

(iv) ferrocenylcorrole complexes.

Chapter One provides a general introduction to the investigated compounds and techniques used in this thesis. Chapter Two discusses the experimental methods and chemicals used in the studies. In Chapter Three, the acid-base and electrochemical properties of free-base porphyrins with pyridyl substituents are discussed, while the acid-base and electrochemical properties of metallopyridylporphyrins are described in Chapter Four. Chapter Five reports the electrochemistry of tetra-*N*-methylpyridylporphyrins with different anions in nonaqueous media. Chapter Six focuses on the electrochemistry of iron ferrocenylcorroles in PhCN.

1.2 Porphyrins

Porphyrins and porphyrinoids have unique physical and chemical properties, which allow for a wide range of applications in the fields of material science, medicine and biology.¹⁻⁵ The basic structural feature of a porphyrin is the tetrapyrrole macrocyclic ring system. The parent porphyrin without substituents is known as porphine (shown in

Chart 1-1). The four nitrogens in the central cavity of porphyrins (and porphines) can bind with most transition and main group metal ions. The porphyrin ring structure is aromatic, with a total of 26 π electrons in the conjugated system. The four pyrrole rings are connected via single-carbon methine bridges. The pyrrole ring is structured with a basic four-fold symmetry, including four nitrogen atoms directed toward the center.

There are 12 positions on the peripheral porphyrin ring (see labeling in Chart 1-1) which may contain different electron-withdrawing or electron-donating substituents. These 12 positions are generally divided into two groups: four *meso* positions (labeled as 5, 10, 15 and 20 in Chart 1-1) and eight β -positions (labeled as 2, 3, 7, 8, 12, 13 and 17, 18). The electron density at the *meso* and β -positions of the macrocycle are proportional to the atomic orbital (AO) coefficients of the porphyrin. According to Gouterman and coworkers,^{6,7} the electron density distribution on the porphyrin HOMO depends on the highest occupied molecular orbital, which has been classified as a_{1u} or a_{2u} . Substituents around the π -ring system will modify the HOMO and LUMO energy levels of the porphyrin π -ring system by electronic perturbation and steric effects. Interaction between substituents, or between the porphyrin ring and bulky substituents, will decrease the conjugation of the π -ring system.^{8,9} Therefore, the chemical and electrochemical properties of porphyrins can be influenced by structural, electronic and steric effects.¹⁰⁻¹⁴

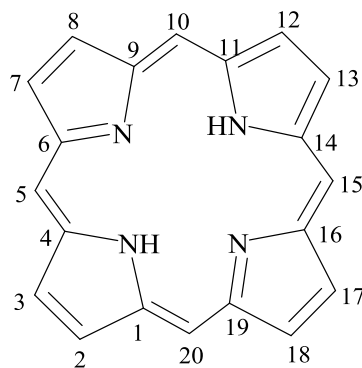


Chart 1-1. Structure of porphyrin (porphine) and labeling system.

The free-base porphyrin ligand, H_2TPP , has a charge of -2. The neutral free-base porphyrin contains two protons bound to the core nitrogens and can accept two more protons to give the diprotonated species $[H_4TPP]^{2+}$. Compounds possessing pyridyl groups on the *meso*-positions of the macrocycle makes the protonation process more complex since proton addition can occur at both the central nitrogen and at the periphery of the molecule. Elucidating the electrochemical and spectroscopic properties of these partially or fully protonated compounds is important for obtaining a clearer understanding of their potential biomedical applications.¹⁵⁻¹⁸

1.3 Pyridylporphyrins and Tetra-4-*N*-Methylpyridylporphyrins

Acid-base properties of simple porphyrins are limited to the protonation or deprotonation of the central nitrogen atoms in the macrocycle. Both of these processes lead to an increase in symmetry from D_{2h} to D_{4h} , and only two Q band absorptions are observed. However, when the peripheral substituents are acidic or basic, it becomes important to determine the relative acidities and basicities of the different sites on the molecule. It is also important to understand the potential interactions which occur

between the sites.¹⁹⁻²² The protonation of free-base pyridylporphyrins in nonaqueous media was reported by Wang and Wamser,²³ but it was unclear from this study whether the central nitrogen atoms and pyridyl substituents were protonated together or separately. As part of our research, we wished to investigate the sequence of protonation processes for several pyridylporphyrins and to also investigate the effect of protonation on the electrochemical properties of the compounds.

Meso-tetrapyridylporphyrins are precursors in the synthesis of tetra-4-*N*-methylpyridylporphyrins. Porphyrins of the type (TMPyP)*M* (shown in Chart 1-2) can be prepared by methylation of the *meso*-pyridyl groups on the tetrakis(4-pyridyl)porphyrin^{24,25} and are generally called “water-soluble” porphyrins due to the positively charged N-CH₃ pyridyl group at each *meso* position of the macrocycle. These porphyrins possess unique electrochemical²⁶⁻³⁵ and physicochemical³⁶⁻⁴¹ properties as a result of their positive charges.

Electrochemistry has been reported for metal derivatives of *N*-methylpyridylporphyrins. However, there are only a few publications on free-base *N*-methylpyridylporphyrins. This is addressed in the present thesis which reports the electrochemistry of positively-charged free-base *N*-methylpyridylporphyrins with different counteranions in nonaqueous solvents.

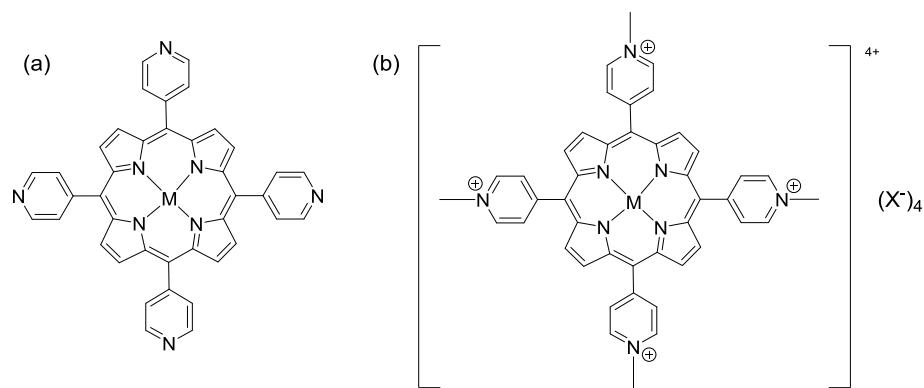


Chart 1-2. Structures of (a) a *meso*-tetrapyrrolylporphyrin and (b) a positively charged tetra-*N*-methylpyridylporphyrin (TMPyP) where the X⁻ counteranions are shown as dissociated.

1.4 Corroles

Corroles are aromatic organic molecules whose structure is similar to a corrin.⁴² The ring consists of nineteen ring carbon atoms, with four nitrogen atoms in the core of the molecule (shown in Chart 1-3). From this perspective, the structure of the corrole is similar to a porphyrin (Chart 1-1), which is also an organic macrocycle but has twenty ring carbon atoms and is found in hemoglobin and chlorophyll. However, corroles and porphyrins differ in the charge of the deprotonated macrocycle, which is -3 for the corrole and -2 for the porphyrin. As a consequence, the corrole macrocycle can stabilize the central metal ion in a higher oxidation state than for the same corresponding metal ion in the porphyrin macrocycle.⁴³ Corroles have attracted considerable interest because of their possible applications in the areas of catalysis,⁴⁴⁻⁵⁵ photochemistry⁵⁶⁻⁷² and pharmacology.⁷³⁻⁸²

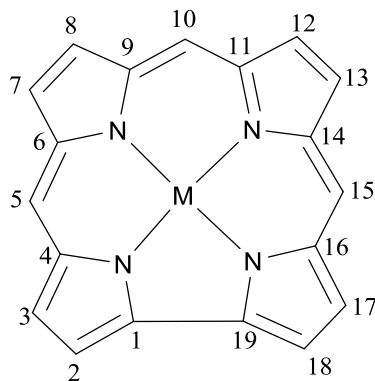


Chart 1-3. Structure and labeling system of a corrole. For comparison, see the core porphyrin structure and labeling system in Chart 1-1.

1.5 Electrochemistry and Spectroelectrochemistry

1.5.1 UV-Vis Spectroscopic Characterization of Porphyrins

The highly conjugated porphyrin macrocycle exhibits an intense absorption (extinction coefficient $> 200,000$) at around 400 nm (the "Soret" band).⁶ There are also several weaker absorptions (Q bands) at longer wavelengths (450 to 700 nm).

1.5.2 Electrochemistry

The electrochemistry of porphyrins, corroles and related molecules has been studied for many years by the Kadish research group.⁸³⁻¹⁰⁰ Cyclic voltammetry has often been utilized to study electrochemical processes and to characterize electron transfer mechanisms and redox potentials, as well as to identify the presence of intermediates in redox reactions. Cyclic voltammetry also can be used as an identification tool for identifying homogenous chemical reactions coupled to the electron transfer and for confirming coordination at the central metal. It is also used to evaluate the number of

electrons added in each redox process and to measure the electrochemical standard potential, called a half wave potential ($E_{1/2}$).

The current-voltage curve in Figure 1-1 illustrates the shape of a cyclic voltammogram. When the potential is scanned negatively from point "a" to point "c", a reduction occurs at the half wave potential of the compound. The resulting current upon reduction is called the cathodic current (i_{pc}). The corresponding peak potential is called the cathodic peak potential (E_{pc}). At point "c" the potential scan is reversed and an oxidation of the reduced species will occur on the back scan. The reverse anodic peak potential is called the anodic peak potential, E_{pa} . The half-wave potential $E_{1/2}$ is determined by the average of E_{pa} and E_{pc} , as shown in Eq 1.1.

$$E_{1/2} = \frac{E_{pa} + E_{pc}}{2} \quad \text{Eq 1.1}$$

The use of electrochemical techniques has made it possible to control redox reactions, to generate new species in high or low oxidation states and to obtain detailed information about the entire electron transfer process, including the reaction mechanisms and the rates of electron transfer.⁸³ In an electrochemical experiment, the LUMO represents the orbital to which an electron is added (reduction) and the HOMO represents the orbital to which an electron is abstracted (oxidation). Therefore, the difference between the first oxidation and the first reduction potential, $|E_{1/2}(\text{ox}) - E_{1/2}(\text{red})|$, can be related to the HOMO-LUMO gap which is also called the "electrochemical gap."¹⁰¹ This piece of data provides a significant link between electrochemical, spectroscopic and structural properties of the molecule. In particular, it provides electrochemical evidence for the degree of π -conjugation in systems such as porphyrins. It may also provide

information about the location of the added or abstracted electron in the singly reduced or singly oxidized species.

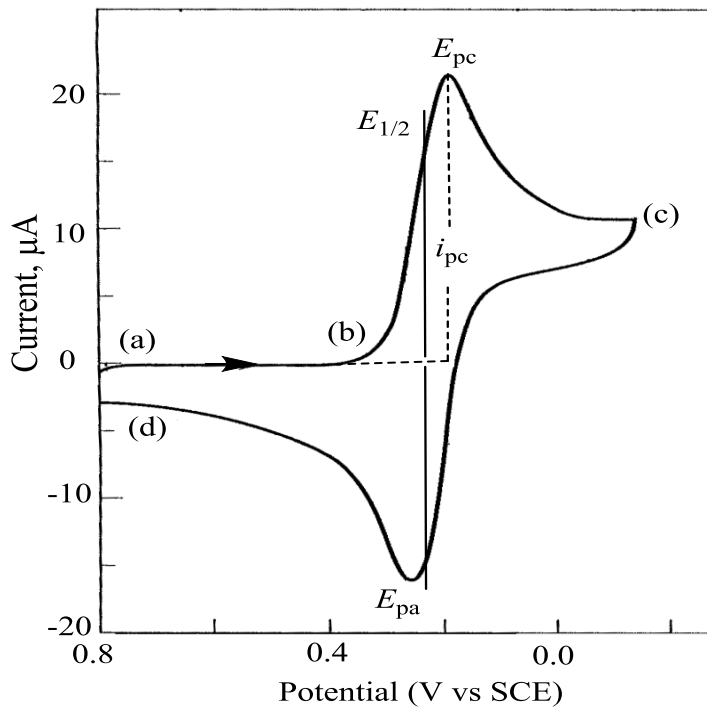


Figure 1-1. Example of cyclic voltammogram showing an initial reduction and reoxidation on the reverse scan.

1.5.3 Spectroelectrochemistry

Spectroelectrochemistry is a method which combines both electrochemical and spectroscopic monitoring techniques. Under potential control, spectroscopic information about *in situ* electrogenerated species may be obtained. The wavelengths and molar absorptivities of the oxidized or reduced products can then be utilized to study electron

transfer mechanisms of a given redox reaction, to identify the products of the redox reaction and, in some cases, to elucidate the site of the electron transfer reaction.

Changes in UV-visible spectra upon oxidation or reduction can provide important information for assigning the site of electron transfer in porphyrins and also for investigating the electronic structure of the oxidized or reduced species. The electronic absorption spectra of metalloporphyrins are dominated by π - π^* transitions.⁶ Therefore, the addition or removal of electrons from the π -ring system of the porphyrin macrocycle will usually lead to major spectral changes. The formation of a porphyrin π -cation radical involves the removal of an electron from the HOMO and transitions from lower lying orbitals to the newly established 'hole' are possible. The UV-visible spectrum of a porphyrin π -radical cation generally consists of broad overlapping bands in the visible region of the spectrum and a broadened and decreased intensity "Soret band" in the spectral region from 380 to 420 nm.

The addition of an electron to the porphyrin LUMO results in the formation of a π -radical anion. The resulting UV-visible spectra are characterized by a collapse of the Soret band to about half of its original intensity and the appearance of visible bands at 600-900 nm.^{6,102,103}

1.6 References

- (1) Chou, J.-h.; Kosal, M. E.; Nalwa, H. S.; Rakow, N. A.; Suslick, K. S.; Academic Press: 2000; Vol. 6, p 43.
- (2) Gust, D.; Moore, T. A.; Academic Press: 2000; Vol. 8, p 153.
- (3) Harvey, P. D.; Elsevier Science: 2003; Vol. 18, p 63.
- (4) Latos-Grazynski, L.; Academic Press: 2000; Vol. 2, p 361.
- (5) Pandey, R. K.; Zheng, G.; Academic Press: 2000; Vol. 6, p 157.
- (6) Gouterman, M. *J. Mol. Spectrosc.* **1961**, *6*, 138.
- (7) Gouterman, M.; Wagniere, G.; Snyder, L. C. *J. Mol. Spectrosc.* **1963**, *11*, 108.
- (8) Meot-Ner, M.; Adler, A. D. *J. Am. Chem. Soc.* **1975**, *97*, 5107.
- (9) Shelnutz, J. A.; Medforth, C. J.; Berber, M. D.; Barkigia, K. M.; Smith, K. *M. J. Am. Chem. Soc.* **1991**, *113*, 4077.
- (10) Cui, Y.; Zeng, L.; Fang, Y.; Zhu, J.; Xu, H.-J.; Desbois, N.; Gros, C. P.; Kadish, K. M. *ChemElectroChem* **2016**, *3*, 110.
- (11) Terazono, Y.; Kodis, G.; Chachisvilis, M.; Cherry, B. R.; Fournier, M.; Moore, A.; Moore, T. A.; Gust, D. *J. Am. Chem. Soc.* **2015**, *137*, 245.
- (12) Bhyrappa, P.; Arunkumar, C.; Varghese, B. *Inorg. Chem.* **2009**, *48*, 3954.
- (13) Puttaiah, B.; Karunanithi, K. *J. Chem. Sci. (Berlin, Ger.)* **2016**, *128*, 501.
- (14) Kumar, R.; Sankar, M. *Inorg. Chem.* **2014**, *53*, 12706.
- (15) Bagherzadeh, M.; Mortazavi-Manesh, A. *RSC Adv.* **2016**, *6*, 41551.
- (16) Gibson, L. E.; Wright, D. W. *Anal. Chem. (Washington, DC, U. S.)* **2016**, Ahead of Print.
- (17) Kumar, R. S.; Jeong, H.; Jeong, J.; Chitumalla, R. K.; Ko, M. J.; Kumar, K. S.; Jang, J.; Son, Y.-A. *RSC Adv.* **2016**, *6*, 41294.
- (18) Pederson, M. R.; Baruah, T.; Kao, D.-y.; Basurto, L. *J. Chem. Phys.* **2016**, Ahead of Print.
- (19) Weinkauff, J. R.; Cooper, S. W.; Schweiger, A.; Wamser, C. C. *The Journal of Physical Chemistry A* **2003**, *107*, 3486.
- (20) Wasbotten, I. H.; Conradie, J.; Ghosh, A. *The Journal of Physical Chemistry B* **2003**, *107*, 3613.
- (21) Ojadi, E. C. A.; Linschitz, H.; Gouterman, M.; Walter, R. I.; Lindsey, J. S.; Wagner, R. W.; Droupadi, P. R.; Wang, W. *The Journal of Physical Chemistry* **1993**, *97*, 13192.
- (22) Walter, R. I.; Ojadi, E. C. A.; Linschitz, H. *The Journal of Physical Chemistry* **1993**, *97*, 13308.
- (23) Wang, C.; Wamser, C. C. *J. Phys. Chem. A* **2014**, *118*, 3605.
- (24) Fleischer, E. B. *Inorg. Chem.* **1962**, *1*, 493.
- (25) Hambright, P.; Fleisher, E. B. *Inorg. Chem.* **1970**, *9*, 1757.
- (26) Yellappa, S.; Seetharamappa, J.; Rogers, L. M.; Chitta, R.; Singhal, R. P.; D'Souza, F. *Bioconjugate Chem.* **2006**, *17*, 1418.
- (27) Trofimova, N. S.; Safronov, A. Y.; Ikeda, O. *Inorg. Chem.* **2003**, *42*, 1945.
- (28) Bell, S. R.; Groves, J. T. *J. Am. Chem. Soc.* **2009**, *131*, 9640.

- (29) Kubat, P.; Sebera, J.; Zalis, S.; Langmaier, J.; Fuciman, M.; Polivka, T.; Lang, K. *Phys. Chem. Chem. Phys.* **2011**, *13*, 6947.
- (30) Weitner, T.; Budimir, A.; Kos, I.; Batinic-Haberle, I.; Birus, M. *Dalton Trans.* **2010**, *39*, 11568.
- (31) Chen, S. M.; Chiu, S. W. *Electrochim. Acta* **2000**, *45*, 4399.
- (32) Kadish, K. M.; Liu, Y. H.; Sazou, D.; Senglet, N.; Guillard, R. *Anal. Chim. Acta* **1991**, *251*, 47.
- (33) Van Caemelbecke, E.; Kutner, W.; Kadish, K. M. *Inorg. Chem.* **1993**, *32*, 438.
- (34) Van Caemelbecke, E.; Derbin, A.; Hambright, P.; Garcia, R.; Doukkali, A.; Saoiabi, A.; Ohkubo, K.; Fukuzumi, S.; Kadish, K. M. *Inorg. Chem.* **2005**, *44*, 3789.
- (35) Kadish, K. M.; Sazou, D.; Liu, Y. M.; Saoiabi, A.; Ferhat, M.; Guillard, R. *Inorg. Chem.* **1988**, *27*, 686.
- (36) Batinic-Haberle, I.; Spasojevic, I.; Stevens, R. D.; Hambright, P.; Fridovich, I. *J. Chem. Soc., Dalton Trans.* **2002**, 2689.
- (37) Lieb, D.; Zahl, A.; Shubina, T. E.; Ivanovic-Burmazovic, I. *J. Am. Chem. Soc.* **2010**, *132*, 7282.
- (38) Aly, S. M. B.; Eita, M.; Khan, J. I.; Alarousu, E.; Mohammed, O. F. *J. Phys. Chem. C* **2014**, *118*, 12154.
- (39) Castriciano, M. A.; Samperi, M.; Camiolo, S.; Romeo, A.; Monsu Scolaro, L. *Chem. - Eur. J.* **2013**, *19*, 12161.
- (40) Schnepfensieper, T.; Zahl, A.; van Eldik, R. *Angew. Chem., Int. Ed.* **2001**, *40*, 1678.
- (41) Xiao, X.; Sun, J.; Jiang, J. *Chem. - Eur. J.* **2013**, *19*, 16891.
- (42) Hitchcock, P. B.; McLaughlin, G. M. *J. Chem. Soc., Dalton Trans.* **1976**, 1927.
- (43) Kadish, K. M.; Erben, C.; Ou, Z.; Adamian, V. A.; Will, S.; Vogel, E. *Inorg. Chem.* **2000**, *39*, 3312.
- (44) Ziegler, J.; Bergman, R. G.; Arnold, J.; American Chemical Society: 2016, p INOR.
- (45) Schoefberger, W.; Faschinger, F.; Chattopadhyay, S.; Bhakta, S.; Mondal, B.; Elemans, J. A. A. W.; Muellegger, S.; Tebi, S.; Koch, R.; Klappenberger, F.; Paszkiewicz, M.; Barth, J. V.; Rauls, E.; Aldahhak, H.; Schmidt, W. G.; Dey, A. *Angew. Chem., Int. Ed.* **2016**, *55*, 2350.
- (46) Kwong, K. W.; Chen, T.-H.; Luo, W.; Malone, J.; Zhang, R.; American Chemical Society: 2015, p SERMACS.
- (47) Avidan-Shlomovich, S.; Gross, Z. *Dalton Trans.* **2015**, *44*, 12234.
- (48) Chen, T.-H.; Kwong, K. W.; Carver, A.; Luo, W.; Zhang, R. *Appl. Catal., A* **2015**, *497*, 121.
- (49) Lei, H.; Fang, H.; Han, Y.; Lai, W.; Fu, X.; Cao, R. *ACS Catal.* **2015**, *5*, 5145.
- (50) Levy, N.; Mahammed, A.; Kosa, M.; Major, D. T.; Gross, Z.; Elbaz, L. *Angew. Chem., Int. Ed.* **2015**, *54*, 14080.
- (51) Tang, J.; Ou, Z.; Ye, L.; Yuan, M.; Fang, Y.; Xue, Z.; Kadish, K. M. *J. Porphyrins Phthalocyanines* **2014**, *18*, 891.

- (52) Wang, Z.; Lei, H.; Cao, R.; Zhang, M. *Electrochim. Acta* **2015**, *171*, 81.
- (53) Ye, L.; Ou, Z.; Meng, D.; Yuan, M.; Fang, Y.; Kadish, K. M. *Turk. J. Chem.* **2014**, *38*, 994.
- (54) Zhu, C.; Cao, Z.-x. *Fenzi Kexue Xuebao* **2014**, *30*, 265.
- (55) Zou, H.-B.; Yang, H.; Liu, Z.-Y.; Mahmood, M. H. R.; Mei, G.-Q.; Liu, H.-Y.; Chang, C.-K. *Organometallics* **2015**, *34*, 2791.
- (56) Edwards, N. Y.; Eikey, R. A.; Khan, S. I.; Abu-Omar, M. M.; American Chemical Society: 2004, p INOR.
- (57) Flamigni, L.; Ciuciu, A. I.; Langhals, H.; Bock, B.; Gryko, D. T. *Chem Asian J* **2012**, *7*, 582.
- (58) Flamigni, L.; Wyrostek, D.; Voloshchuk, R.; Gryko, D. T. *Phys. Chem. Chem. Phys.* **2010**, *12*, 474.
- (59) Giribabu, L.; Kandhadi, J.; Kanaparthi, R. K.; Kanaparthi, R. K. *J Fluoresc* **2014**, *24*, 569.
- (60) Grodkowski, J.; Neta, P.; Fujita, E.; Mahammed, A.; Simkhovich, L.; Gross, Z. *J. Phys. Chem. A* **2002**, *106*, 4772.
- (61) Harischandra, D. N.; Zhang, R.; Newcomb, M. *J. Am. Chem. Soc.* **2005**, *127*, 13776.
- (62) Kandhadi, J.; Yeduru, V.; Bangal, P. R.; Giribabu, L. *Phys. Chem. Chem. Phys.* **2015**, *17*, 26607.
- (63) Kandhadi, J.; Yeduru, V.; Bangal, P. R.; Giribabu, L. *Phys Chem Chem Phys* **2015**, *17*, 26607.
- (64) Murakami, Y.; Aoyama, Y.; Tokunaga, K. *J. Chem. Soc., Chem. Commun.* **1979**, 1018.
- (65) Paolesse, R.; Sagone, F.; Macagnano, A.; Boschi, T.; Prodi, L.; Montalti, M.; Zaccheroni, N.; Bolletta, F.; Smith, K. M. *J. Porphyrins Phthalocyanines* **1999**, *3*, 364.
- (66) Reith, L. M.; Himmelsbach, M.; Schoefberger, W.; Knoer, G. *J. Photochem. Photobiol., A* **2011**, *218*, 247.
- (67) Reith, L. M.; Stifftinger, M.; Monkowius, U.; Knoer, G.; Schoefberger, W. *Inorg. Chem.* **2011**, *50*, 6788.
- (68) Shi, L.; Liu, H.-Y.; Peng, K.-M.; Wang, X.-L.; You, L.-L.; Lu, J.; Zhang, L.; Wang, H.; Ji, L.-N.; Jiang, H.-F. *Tetrahedron Lett.* **2010**, *51*, 3439.
- (69) Swider, P.; Nowak-Krol, A.; Voloshchuk, R.; Lewtak, J. P.; Gryko, D. T.; Danikiewicz, W. *J. Mass Spectrom.* **2010**, *45*, 1443.
- (70) Zhang, R.; Harischandra, D. N.; Newcomb, M. *Chem. - Eur. J.* **2005**, *11*, 5713.
- (71) Barata, J. F. B.; Faustino, M. A. F.; Tome, A. C.; Cavaleiro, J. A. S.; Zamarron, A.; Juarranz, A.; Neves, M. G. P. M. S.; Roder, B.; Sanz-Rodriguez, F. *Eur J Med Chem* **2015**, *92*, 135.
- (72) Haber, A.; Aviram, M.; Gross, Z. *Inorg Chem* **2012**, *51*, 28.
- (73) Hwang, J. Y.; Lubow, D. J.; Sims, J. D.; Gray, H. B.; Mahammed, A.; Gross, Z.; Medina-Kauwe, L. K.; Farkas, D. L. *J Biomed Opt* **2012**, *17*, 015003.
- (74) Hwang, J. Y.; Lubow, J.; Chu, D.; Ma, J.; Agadjanian, H.; Sims, J.; Gray, H. B.; Gross, Z.; Farkas, D. L.; Medina-Kauwe, L. K. *Mol Pharm* **2011**, *8*, 2233.

- (75) Kanamori, A.; Catrinescu, M.-M.; Mahammed, A.; Gross, Z.; Levin, L. A. *J Neurochem* **2010**, *114*, 488.
- (76) Kupersmidt, L.; Okun, Z.; Amit, T.; Mandel, S.; Saltsman, I.; Mahammed, A.; Bar-Am, O.; Gross, Z.; Youdim, M. B. H. *J Neurochem* **2010**, *113*, 363.
- (77) Nigel-Etinger, I.; Mahammed, A.; Gross, Z. *Catal. Sci. Technol.* **2011**, *1*, 578.
- (78) Okun, Z.; Kupersmidt, L.; Amit, T.; Mandel, S.; Bar-Am, O.; Youdim, M. B. H.; Gross, Z. *ACS Chem Biol* **2009**, *4*, 910.
- (79) Preuss, A.; Saltsman, I.; Mahammed, A.; Pfitzner, M.; Roder, B.; Goldberg, I.; Gross, Z. *J Photochem Photobiol B* **2014**, *133*, 39.
- (80) Teo, R. D.; Gray, H. B.; Lim, P.; Termini, J.; Domeshek, E.; Gross, Z. *Chem Commun (Camb)* **2014**, *50*, 13789.
- (81) Kadish, K. M.; Van Caemelbecke, E.; Royal, G.; Academic Press: 2000; Vol. 8, p 1.
- (82) Autret, M.; Ou, Z.; Antonini, A.; Boschi, T.; Tagliatesta, P.; Kadish, K. M. *J. Chem. Soc., Dalton Trans.* **1996**, 2793.
- (83) D'Souza, F.; Villard, A.; Van Caemelbecke, E.; Franzen, M.; Boschi, T.; Tagliatesta, P.; Kadish, K. M. *Inorg. Chem.* **1993**, *32*, 4042.
- (84) Fukuzumi, S.; Ohkubo, K.; Imahori, H.; Shao, J.; Ou, Z.; Zheng, G.; Chen, Y.; Pandey, R. K.; Fujitsuka, M.; Ito, O.; Kadish, K. M. *J. Am. Chem. Soc.* **2001**, *123*, 10676.
- (85) Ghosh, A.; Halvorsen, I.; Nilsen, H. J.; Steene, E.; Wondimagegn, T.; Lie, R.; van Caemelbecke, E.; Guo, N.; Ou, Z.; Kadish, K. M. *J. Phys. Chem. B* **2001**, *105*, 8120.
- (86) Guilard, R.; Gros, C. P.; Barbe, J.-M.; Espinosa, E.; Jerome, F.; Tabard, A.; Latour, J.-M.; Shao, J.; Ou, Z.; Kadish, K. M. *Inorg. Chem.* **2004**, *43*, 7441.
- (87) Guilard, R.; Perie, K.; Barbe, J.-M.; Nurco, D. J.; Smith, K. M.; Van Caemelbecke, E.; Kadish, K. M. *Inorg. Chem.* **1998**, *37*, 973.
- (88) Kadish, K. M. *Prog. Inorg. Chem.* **1986**, *34*, 435.
- (89) Kadish, K. M.; Autret, M.; Ou, Z.; Tagliatesta, P.; Boschi, T.; Fares, V. *Inorg. Chem.* **1997**, *36*, 204.
- (90) Kadish, K. M.; Fremond, L.; Ou, Z.; Shao, J.; Shi, C.; Anson, F. C.; Burdet, F.; Gros, C. P.; Barbe, J.-M.; Guilard, R. *J. Am. Chem. Soc.* **2005**, *127*, 5625.
- (91) Kadish, K. M.; Fremond, L.; Shen, J.; Chen, P.; Ohkubo, K.; Fukuzumi, S.; El Ojaimi, M.; Gros, C. P.; Barbe, J.-M.; Guilard, R. *Inorg. Chem.* **2009**, *48*, 2571.
- (92) Kadish, K. M.; Guo, N.; Van Caemelbecke, E.; Froiio, A.; Paolesse, R.; Monti, D.; Tagliatesta, P.; Boschi, T.; Prodi, L.; Bolletta, F.; Zaccheroni, N. *Inorg. Chem.* **1998**, *37*, 2358.
- (93) Kadish, K. M.; Ou, Z.; Shao, J.; Gros, C. P.; Barbe, J.-M.; Jerome, F.; Bolze, F.; Burdet, F.; Guilard, R. *Inorg. Chem.* **2002**, *41*, 3990.
- (94) Kadish, K. M.; Shao, J.; Ou, Z.; Comte, C.; Gros, C. P.; Guilard, R. *J. Porphyrins Phthalocyanines* **2000**, *4*, 639.
- (95) Kadish, K. M.; Shao, J.; Ou, Z.; Fremond, L.; Zhan, R.; Burdet, F.; Barbe, J.-M.; Gros, C. P.; Guilard, R. *Inorg. Chem.* **2005**, *44*, 6744.

- (96) Kadish, K. M.; Van Caemelbecke, E.; D'Souza, F.; Medforth, C. J.; Smith, K. M.; Tabard, A.; Guilard, R. *Inorg. Chem.* **1995**, *34*, 2984.
- (97) Richter-Addo, G. B.; Hodge, S. J.; Yi, G.-B.; Khan, M. A.; Ma, T.; Van Caemelbecke, E.; Guo, N.; Kadish, K. M. *Inorg. Chem.* **1996**, *35*, 6530.
- (98) Beer, P. D.; Gale, P. A.; Chen, G. Z. *Coordination Chemistry Reviews* **1999**, *185–186*, 3.
- (99) Anderson, H. L. *Chem. Commun. (Cambridge)* **1999**, 2323.
- (100) Perrin, M. H.; Gouterman, M.; Perrin, C. L. *J. Chem. Phys.* **1969**, *50*, 4137.
- (101) Fuhrhop, J. H. *Struct. Bonding (Berlin)* **1974**, *18*, 1.

Chapter Two
Experimental Methods

2.1 Cyclic Voltammetry

Cyclic voltammetry was carried out at 298 K using an EG&G Princeton Applied Research (PAR) 173 potentiostat/galvanostat. A home-built three-electrode cell was used for cyclic voltammetric measurements which consists of a glassy carbon working electrode (WE), a platinum counter electrode (CE) and a homemade saturated calomel reference electrode (SCE). The SCE was separated from the bulk of the solution by a fritted glass bridge of low porosity, which contained the solvent/supporting electrolyte mixture. The working and counter electrodes were made from platinum mesh. Both the working and reference electrodes were placed in one compartment, while the counter electrode was in another compartment.

The potential is applied between the working electrode and the reference electrode. Measurements were conducted using a three-electrode cell (Figure 2-1). In cyclic voltammetry, the potential of the working electrode is ramped linearly versus time, as shown in Figure 2-2. In the 1st cycle (solid line), the potential scans negatively, starting from +0.8 V to -0.2 V and then the scan reverses and returns to the initial potential of +0.8 V. The half wave potential for the investigated reaction should be located between +0.8 and -0.2 V for the example given.

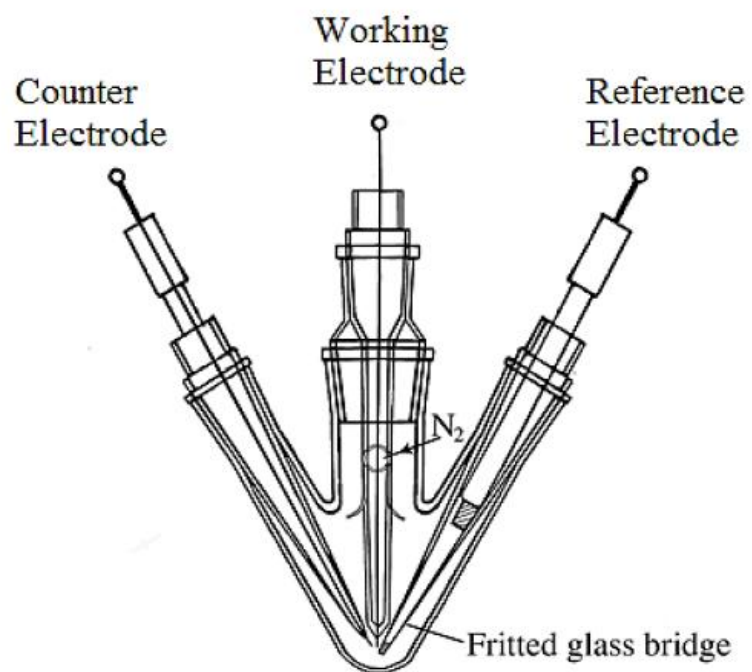


Figure 2-1. Schematic illustration of the home-built electrochemical cell with the working counter and reference electrodes.

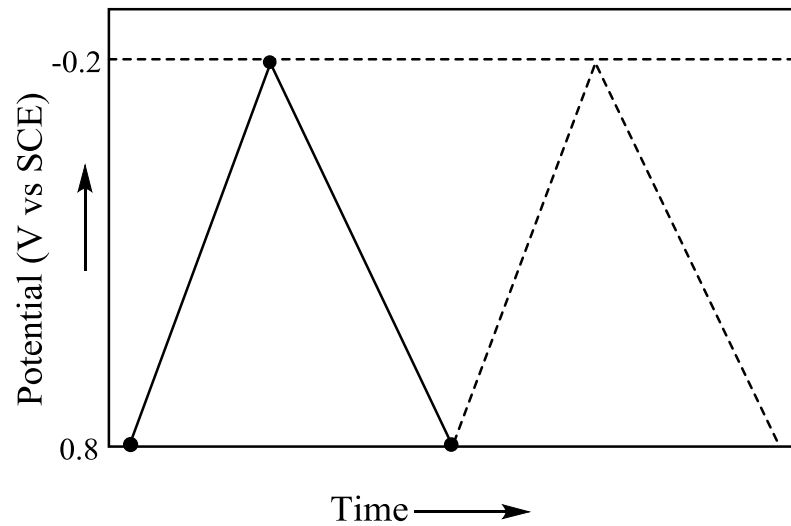


Figure 2-2. Cyclic voltammetry waveform showing a scan between 0.8 to -0.2 V.

2.2 UV-Visible Spectroelectrochemistry Methods

Spectroelectrochemical experiments were performed using a home-built thin-layer cell, which has a platinum net working electrode (Figure 2-3).^{1,2} Potentials were applied and monitored with an EG&G PAR Model 173 potentiostat. High-purity N₂ from Trigas was used to deoxygenate the solution and was kept over the solution during each electrochemical and spectroelectrochemical experiment. Time-resolved UV-visible spectra were recorded with a Hewlett-Packard Model 8453 diode array spectrophotometer. The combination of electrochemistry and spectroscopy allows for a determination of the spectrum of the species formed in solution during the time of the electron transfer. The use of spectroelectrochemistry may help to determine the specific site of electron transfer.

2.3 Spectral Titration Methods For Determination of Equilibrium Constants

Changes in the UV-visible spectra of the pyridylporphyrins in CH₂Cl₂ were monitored during a titration with TFA and the resulting spectral data was then used to calculate the formation constants for proton addition using the Hill equation³

$$\log [(A_i - A_0)/(A_0 - A_f)] = \log K + n \log [H^+]$$

where A_i is the absorbance in solutions with a specific concentration of added protons $[H^+]$, A_0 is the initial absorbance when $[H^+] = 0.0$ and A_f is the final absorbance of the fully protonated porphyrin. The slope of the $\log [(A_i - A_0)/(A_0 - A_f)]$ vs $\log[H^+]$ plot gives n , the number of protons added to the core nitrogen atoms. The value of $\log K$ is evaluated

from the intercept of the line at $\log[(A_i - A_0)/(A_0 - A_f)] = 0.0$. An example of UV-visible spectra changes during a titration is shown in Figure 2-4. This method has been utilized in publications of our group to study protonation/deprotonation or equilibrium constants.⁴⁻⁹

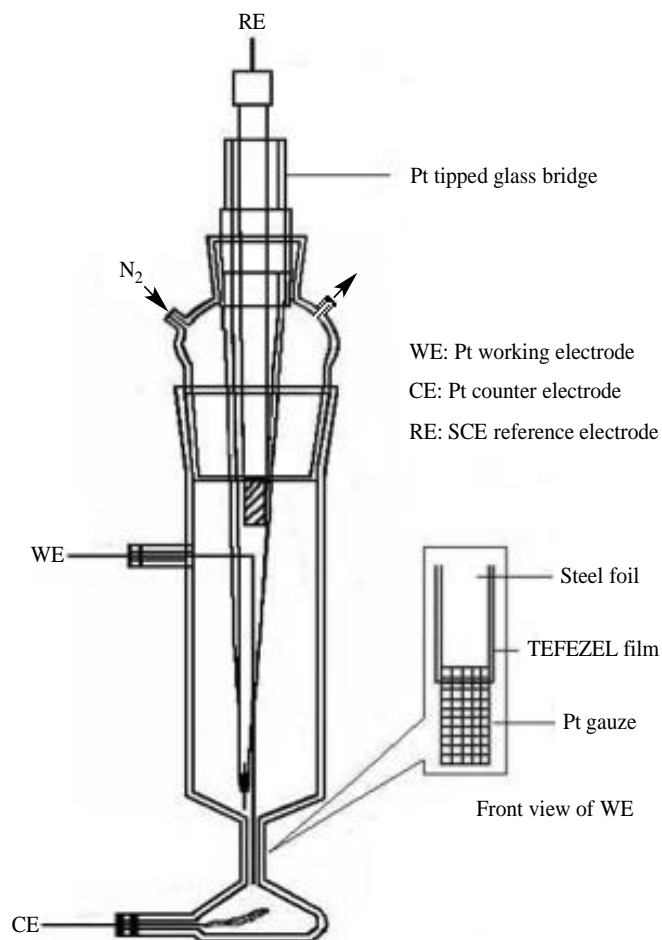


Figure 2-3 Schematic illustration of the thin-layer UV-visible spectroelectrochemical cell.¹

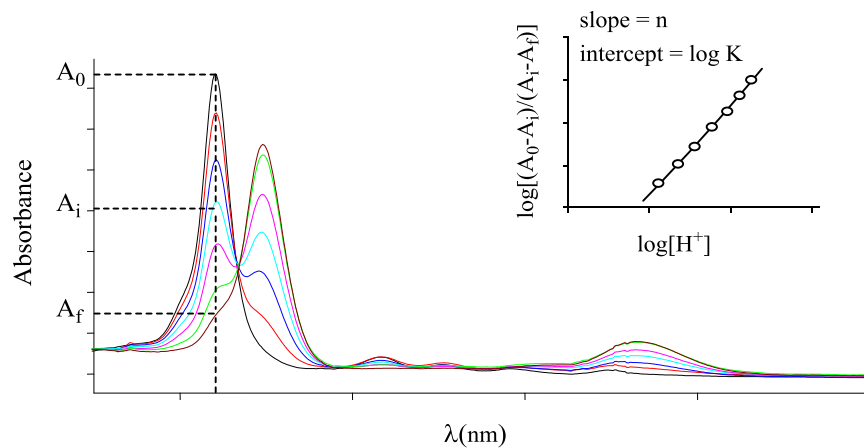


Figure 2-4 An example of UV-visible spectra changes during titration, where A_0 is the initial absorbance, A_i is the absorbance at a given point in the titration and A_f is the absorbance in the final step.

2.4 Other Experimental Methods

2.4.1 Degassing the Solution

High-purity nitrogen (99.99%, Ultra High Purity, Matheson-Trigas) was used to deoxygenate the solutions for 5-10 minutes before each electrochemical experiment and a positive nitrogen pressure was maintained above the solution throughout the experiment.

2.5 Chemicals and Investigated Compounds

2.5.1 Chemicals

Benzonitrile (PhCN) was purchased from Sigma-Aldrich Chemical Co. and distilled over P₂O₅ under vacuum prior to use. Absolute dichloromethane (CH₂Cl₂, 99.8%) from EMD Chemicals Inc. was used for electrochemistry without further purification. N,N'-dimethylformamide (DMF) and dimethyl sulfoxide (DMSO) were purchased from Sigma-Aldrich Chemical Co. High purity N₂ from Matheson-Trigas was used to deoxygenate the solutions for 5-10 minutes before each electrochemical experiment. Tetra-*n*-butylammonium perchlorate (TBAP), tetra-*n*-butylammonium chloride > 97% (TBACl), tetra-*n*-butylammonium bromide > 98% (TBABr) and tetra-*n*-butylammonium iodide > 99% (TBAI), used as supporting electrolyte, were purchased from Sigma-Aldrich.

2.5.2 Investigated Compounds

All compounds investigated in this thesis were synthesized in the laboratories of our collaborators. The free-base and metallopyridylporphyrins (Co, Ni, Cu and Zn) with

one, two or four pyridyl substituents were prepared by Dr. Claude Gros's group at the Université de Bourgogne in Dijon, France. Iron ferrocenylcorroles with NO, C₆H₅ or Cl⁻ as axial ligands were prepared by the group of Dr. Roberto Paolesse at the Università di Roma Tor Vergata in Italy. Free-base tetra-*N*-methylpyridylporphyrins with Cl⁻, Br⁻, I⁻ or PhSO₃⁻ as counter anion were prepared by PorphyChem in Dijon, France. All of the investigated compounds were stored in the dark and, in some cases, under vacuum. The UV-visible spectrum of each compound was measured in Houston before carrying out the experiments and the resulting spectral data was compared to the spectrum provided to us by our collaborators or published in the literature.

2.6 References

- (1) Lin, X. Q.; Kadish, K. M. *Anal. Chem.* **1985**, *57*, 1498.
- (2) Kadish, K. M.; Mu, X. H.; Lin, X. Q. *Electroanalysis (N. Y.)* **1989**, *1*, 35.
- (3) Brault, D.; Rougee, M. *Biochemistry* **1974**, *13*, 4591.
- (4) Feng, R.; Ou, Z.; Xue, Z.; Fang, Y.; Song, Y.; Kadish, K. M. *RSC Adv.* **2015**, *5*, 96769.
- (5) Xue, S.; Ou, Z.; Ye, L.; Lu, G.; Fang, Y.; Jiang, X.; Kadish, K. M. *Chem. - Eur. J.* **2015**, *21*, 2651.
- (6) Fang, Y.; Bhyrappa, P.; Ou, Z.; Kadish, K. M. *Chem. - Eur. J.* **2014**, *20*, 524.
- (7) Ou, Z.; Meng, D.; Yuan, M.; Huang, W.; Fang, Y.; Kadish, K. M. *J. Phys. Chem. B* **2013**, *117*, 13646.
- (8) Ou, Z.; Sun, H.; Zhu, W.; Da, Z.; Kadish, K. M. *J. Porphyrins Phthalocyanines* **2008**, *12*, 1.
- (9) Ou, Z.; Shen, J.; Shao, J.; E, W.; Galezowski, M.; Gryko, D. T.; Kadish, K. M. *Inorg. Chem.* **2007**, *46*, 2775.

Chapter Three

Electrochemistry and Acid-Base Properties of Free-base Pyridylporphyrins in Nonaqueous Media

3.1 Introduction

Equilibrium constants for the conversion of each neutral porphyrin to its diprotic $[H_4P]^{2+}$ form were determined and the electrochemistry was elucidated as a function of: (i) type of nonaqueous solvent, (ii) anion of the supporting electrolyte, (iii) porphyrin ring substituents and (iv) concentration of acid added to solution. Spectroelectrochemistry was used to characterize absorption spectra of each electroreduced species and, when combined with results of the former studies, significantly improves the ability to tune the redox reactivity of these types of compounds.¹⁻³

The protonation properties of two mono-pyridylcorroles, (2, 4, 6-tri-MePh)₂PyCorH₃ and (2, 6-di-ClPh)₂PyCorH₃, and one di-pyridylcorrole, represented as (2, 6-di-F-Ph)Py₂CorH₃, were investigated in 2007 by Kadish and coworkers.⁴ For the mono-pyridylcorroles, the first proton addition occurs at the nitrogen of the *meso*-pyridyl substituents, while the second proton is added to the central nitrogens of the macrocycle. The corrole with two *meso*-pyridyl groups can accept three protons in total, one at the nitrogen of each pyridyl group and one at the unprotonated nitrogen of the macrocycle. The reported pyridyl group protonation constants ranged from 3.25 to 4.34, while the core nitrogen protonation constants ranged from 0.80 to 2.38 in benzonitrile (PhCN), with trifluoroacetic acid (TFA).⁴

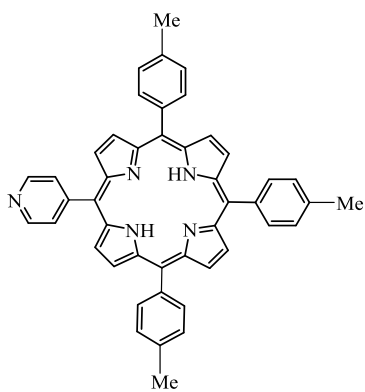
Meso-tetrapyridylporphyrins are precursors in the synthesis of tetra-*N*-methylpyridylporphyrins and many of these compounds have been examined as to their electrochemistry in both water^{9, 12} and nonaqueous solvents.⁵⁻¹² Recently, the protonation

of free-base pyridylporphyrins with zero, one, two (cis and trans), three or four *meso*-pyridyl groups was reported by Wang and Wamser using UV-vis¹³ and NMR¹⁴ spectroscopy to monitor the reactions.

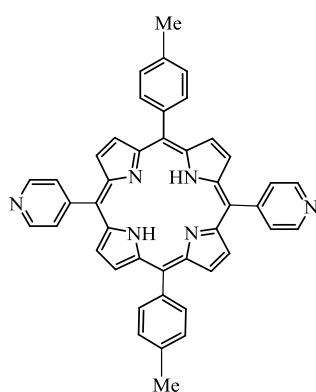
The free-base porphyrin with a *meso*-aminophenyl group interacts with the protonated pyridyl groups of the protonated porphyrins, but no such interaction was observed for the compounds with unsubstituted phenyl substituents.

The role of counteranions in acid-induced aggregation of three different types of isomeric tetrapyrrolylporphyrins were studied by Scolaro and coworkers¹⁰ in organic solvents represented, where the investigated compounds are represented as H₂Py₄Por, H₂Py₃Por and H₂Py₂Por. The UV-vis spectral data confirmed that H₂Py₄Por was first protonated on the four pyridyl groups and then on the porphyrin central nitrogen. The spectroscopic features of the protonated and aggregated porphyrins were strongly influenced by the nature of the acid counterion, which was Cl⁻, Br⁻, I⁻ or CF₃COO⁻.

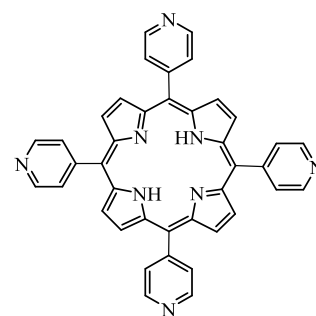
In order to better understand how changes in the *meso*-substituents and the overall charge of a porphyrin might affect protonation of the central and pyridyl nitrogens, we examined the UV-vis spectra and electrochemistry of several free-base and metallo-pyridylporphyrins in neutral and acidic media; the structures of the investigated pyridylporphyrins are shown in Chart 3-1.



$\text{H}_2\text{Py}(\text{PhMe})_3\text{P}$, **1H₂**



$\text{H}_2\text{Py}_2(\text{PhMe})_2\text{P}$, **2H₂**



$\text{H}_2\text{Py}_4\text{P}$, **4H₂**

Chart 3-1. Structures of investigated pyridylporphyrins.

3.2 Results and Discussion

3.2.1 Spectroscopic Characterization

Electronic absorption spectra of $\text{H}_2\text{Py}(\text{PhMe})_3\text{Por}$ **1H₂**, $\text{H}_2\text{Py}_2(\text{PhMe})_2\text{Por}$ **2H₂** and $\text{H}_2\text{Py}_4\text{Por}$ **4H₂** in CH_2Cl_2 and pyridine are illustrated in Figure 3-1 and a summary of the spectral data in the five utilized nonaqueous solvents is given in Table 3-1. Each free-base pyridylporphyrin is characterized by a Soret band at 417 to 423 nm and four Q bands located between 511 and 650 nm. As seen in the table, similar spectral features are present for each neutral compound, independent of the solvent and number of *meso*-pyridyl groups on the compound. Similar UV-visible spectra are also seen for the fully protonated free-base porphyrins in acid media. This spectral data is shown in Table 3-1, where the protonated compounds in DMF are represented in Table 3-2 as $\text{H}_4\text{TPP}^{2+}$, **1H₅³⁺** and **2H₆⁴⁺**.

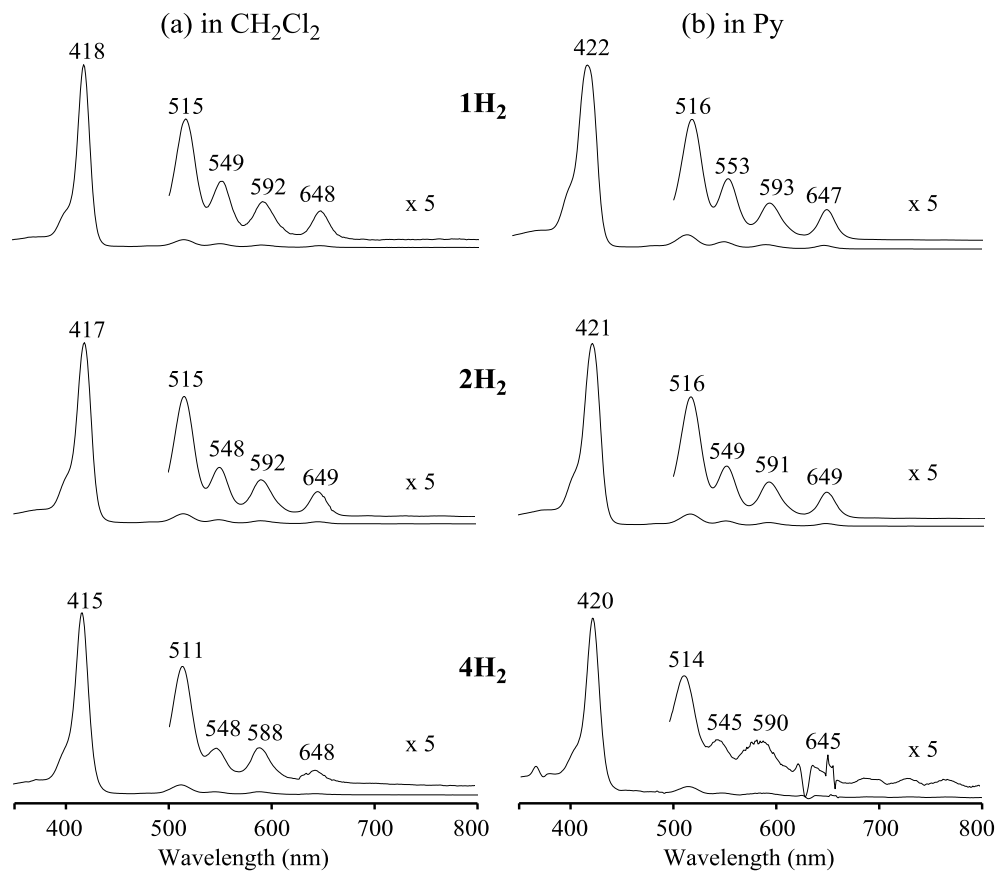


Figure 3-1. UV-vis spectra of investigated free-base pyridylporphyrins in CH_2Cl_2 and pyridine. Values of $\log \epsilon$ are given in **Table 3-1**.

Table 3-1. UV/vis spectra data λ_{max} ($\log \epsilon$), nm for H_2TPP , $\mathbf{1H}_2$, $\mathbf{2H}_2$ and $\mathbf{4H}_2$ in different solvents.

Solvent	compd	Soret band		Q bands		
CH ₂ Cl ₂	H₂TPP	418 (5.41)	515 (4.15)	549 (3.92)	593 (3.08)	649 (3.06)
	1H₂	418 (4.71)	515 (3.64)	551 (3.32)	590 (3.11)	647 (3.04)
	2H₂	420 (4.88)	517 (3.60)	554 (3.29)	593 (3.19)	650 (3.38)
	4H₂	415	511	548	588	648
PhCN	H₂TPP	423 (5.47)	516 (4.13)	552 (3.83)	593 (3.08)	649 (3.06)
	1H₂	423 (4.73)	518 (3.48)	553 (3.20)	593 (2.95)	647 (2.90)
	2H₂	423 (4.81)	518 (3.26)	555 (3.28)	593 (3.09)	649 (3.08)
DMSO	H₂TPP	420 (5.42)	515 (3.97)	549 (3.45)	591 (3.23)	646 (3.08)
	1H₂	419 (4.79)	515 (3.83)	550 (3.52)	591 (3.32)	647 (3.28)
	2H₂	418 (4.70)	515 (3.33)	550 (2.96)	591 (2.85)	647 (2.80)
DMF	H₂TPP	418 (5.41)	515 (4.07)	549 (3.69)	591 (3.51)	646 (3.40)
	1H₂	418 (4.81)	515 (3.87)	550 (3.57)	593 (3.32)	646 (3.30)
	2H₂	417 (5.05)	515 (3.67)	550 (3.25)	595 (3.09)	647 (3.16)
Py	H₂TPP	420 (5.25)	517 (3.96)	550 (3.69)	595 (3.52)	649 (3.54)
	1H₂	422 (5.30)	516 (4.18)	553 (3.70)	593 (3.68)	647 (3.60)
	2H₂	421 (5.37)	516 (4.19)	549 (3.83)	591 (3.68)	649 (3.54)
	4H₂	420	514	545	590	645

Table 3-2. UV-vis spectra data λ_{\max} , nm for $\text{H}_4\text{TPP}^{2+}$, $\mathbf{1H}_5^{3+}$ and $\mathbf{2H}_6^{4+}$ in DMF.

compd	Soret band	Q band
$\text{H}_4\text{TPP}^{2+}$	443	660
$\mathbf{1H}_5^{3+}$	448	669
$\mathbf{2H}_6^{4+}$	446	670

3.2.2 UV-Vis Spectral Monitoring of Free-Base Pyridylporphyrin Protonation

Protonation constants of the pyridylporphyrins were determined by monitoring changes in the UV-visible spectra as H^+ was added to solution in the form of trifluoroacetic acid (TFA). An example of the data is shown in Figure 3-2 for the case of $\text{H}_2\text{Py}(\text{PhMe})_3\text{Por}$ $\mathbf{1H}_2$ in PhCN and DMF. Also included in this figure is data for the reference porphyrin, H_2TPP , in the same solvents.

As seen in Figure 3-2, the protonation of $\mathbf{1H}_2$ occurs in two steps, the first of which involves the addition of one H^+ and the second two H^+ , as indicated by the slopes of the log-log plot. Only a slight red shift in the Soret band position is observed during the first protonation step; the shift in λ_{\max} is 4 nm in PhCN and 3 nm in DMF. The measured first step protonation constant was $\log K = 3.79$ in PhCN and 2.05 in DMF.

Significant spectral changes are observed during the second step protonation, where the Soret band shifts from 427 to 453 nm in PhCN and 421 to 448 nm in DMF. The free-base pyridylporphyrin accepts two protons in the second step and the measured protonation constants were $\log \beta_2 = 3.00$ in PhCN and 0.30 in DMF. The observed

spectral changes and the magnitude of the protonation constant in the second step are similar for **1H₂** and H₂TPP, as shown in Figure 3-2. These results indicate that the first proton is added on the pyridyl group, followed by a two proton addition to the porphyrin central nitrogen atoms, as demonstrated for related compounds in a previous publication.⁴ Even though similar spectral changes are observed for **1H₂** and H₂TPP in PhCN and THF, the protonation constant in DMF is much smaller than in PhCN. This is because DMF is a more basic solvent than PhCN. A summary of the measured protonation constants is given in Table 3-3.

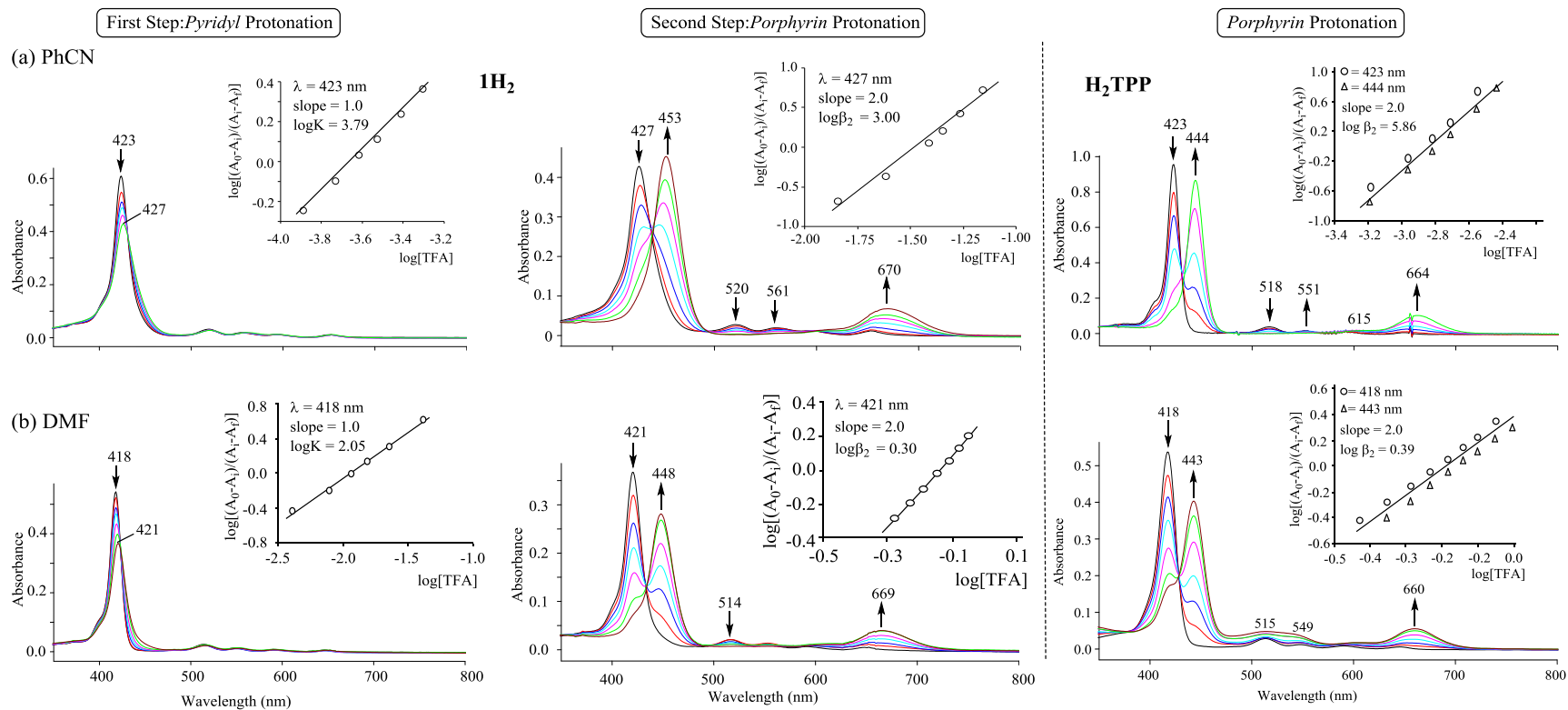


Figure 3-2. UV-vis spectral changes during titration of free-base porphyrins **1H₂** and **H₂TPP** in (a) PhCN and (b) DMF with TFA and analysis of data for calculation of proton addition.

Table 3-3. Protonation constants for mono- and di-pyridyl free-base porphyrins in different solvents.

Solvent	1H₂		2H₂	
	n	logK ₁	n	logK ₁
PhCN	1.0	3.79	1.0	4.31
DMSO	1.0	3.06	1.0	3.06
DMF	1.0	2.05	1.0	1.91

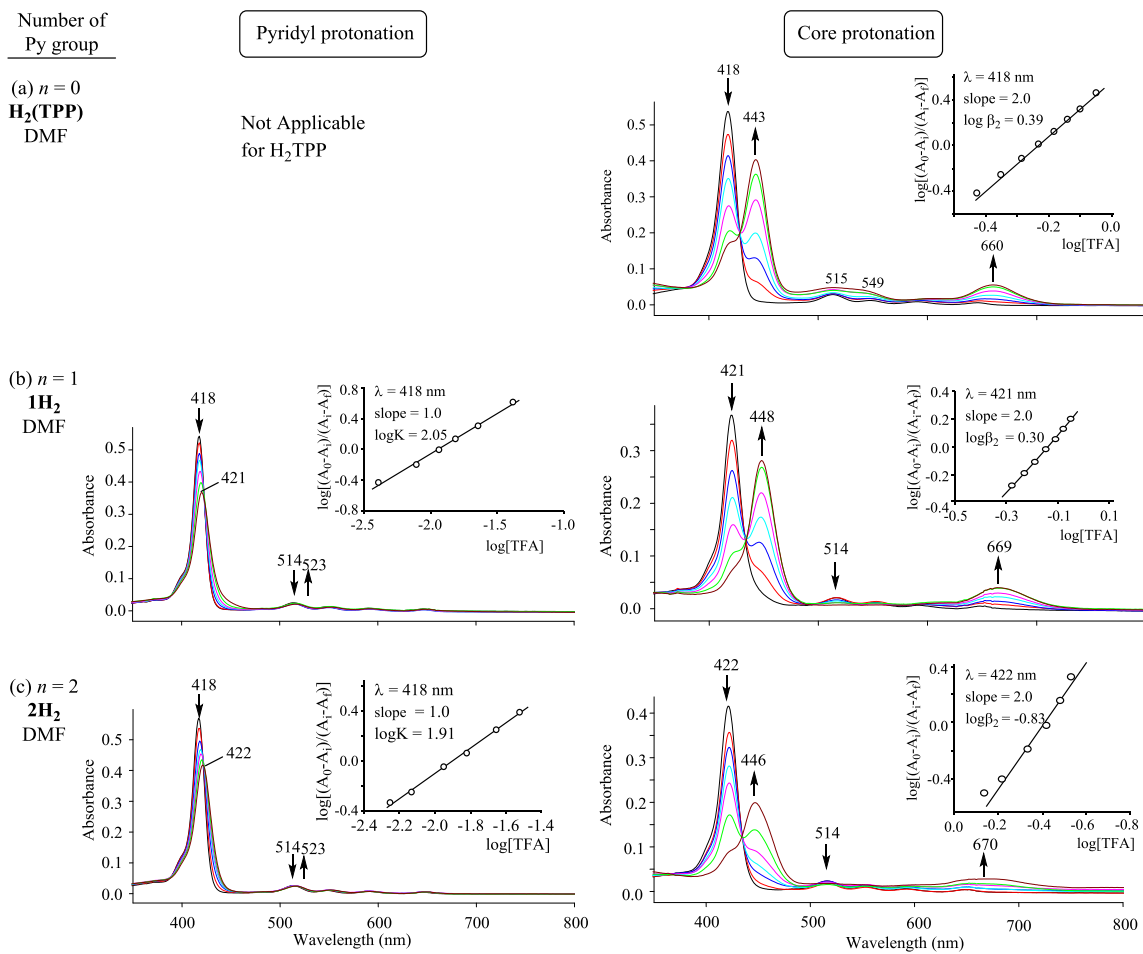


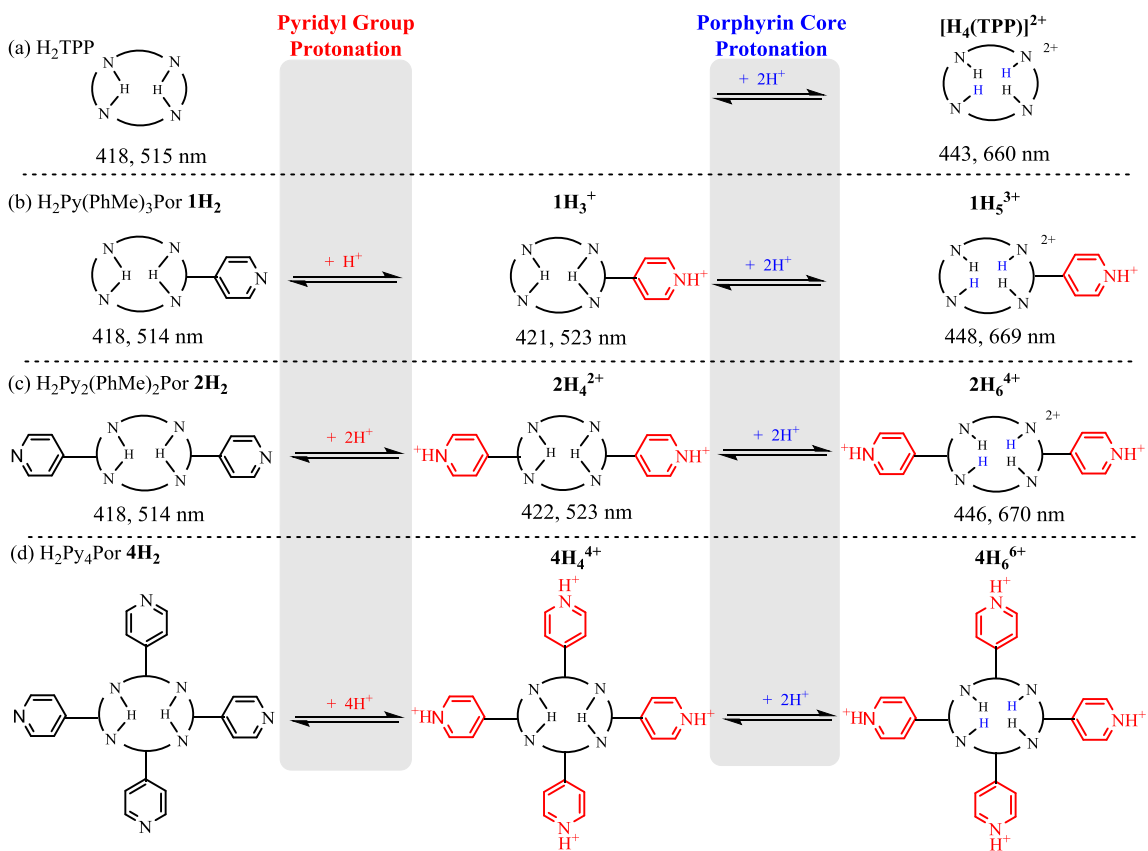
Figure 3-3. UV-vis spectral changes during titration of (a) **H₂TPP**, (b) **1H₂** and (c) **2H₂** with TFA and diagnostic log-log plots for calculation of proton constants.

As seen in Figure 3-3, protonation of the mono- and di-pyridylporphyrins **1H₂** and **2H₂** occurs in two steps. The first proton addition involves the *meso*-pyridyl group(s), giving **1H₃⁺** and **2H₄²⁺**, while the second involves the central nitrogen atoms, giving **1H₅³⁺** and **2H₆⁴⁺**. UV-vis spectra of the protonated pyridyl compounds **1H₃⁺** and **2H₄²⁺** are virtually identical to each other. These spectra are characterized by a Soret band at 421 or 422 nm and a Q band at 523 nm. The logK values are also similar for the two free-base porphyrins, *i.e.*, logK = 2.05 and 1.91, respectively. The similar logK values for pyridyl group(s) protonation and similar spectra for the products of the protonation are consistent with the lack of an interaction between the neutral or protonated pyridyl groups of **2H₂** and **2H₄²⁺** across the molecule. Further evidence for this lack of interaction is given by the slope of 1.0 in the log-log plot of the pyridyl group protonation (see Figure 3-3c), which indicates that one proton is added to each of the two pyridyl nitrogen atoms of **2H₂** at the same time, with no interaction between those two *meso*-substituents across the porphyrin macrocycle.

Protonation of the central nitrogen atoms of **H₂(TPP)**, **1H₂** and **2H₂** occurs via a simultaneous two proton addition, as shown in Scheme 3-1. The final spectrum of **[H₄(TPP)]²⁺** in DMF is characterized by a Soret band at 443 nm and a Q band at 660 nm (Figure 3-3a). This spectrum can be compared to the spectrum of **1H₅³⁺** in the same solvent which has bands at 448 and 669 nm (Figure 3-3b), and **2H₆⁴⁺** which has bands at 446 nm and 670 nm (Figure 3-3c).

The assignment for protonation on the pyridyl groups in the first step is also confirmed by the same type of spectral changes for the mono-pyridyl metalloporphyrins described in Chapter 4. These compounds are represented as **1M**, where M = Cu, Ni and Zn and have the structures shown in Figure 4-1.

Scheme 3-1. Proposed protonation mechanism for free-base pyridylporphyrins.



3.2.3 Protonated Pyridylporphyrins

The spectroscopic properties of protonated tetrapyrrolylporphyrins in acidic nonaqueous media has been examined by several research groups,¹⁵⁻¹⁷ but the electrochemistry of these compounds has not been examined in previous studies and is therefore addressed in the current thesis.

Cyclic voltammograms of the mono- and di-pyridylporphyrins are shown in Figure 3-4 before and after the addition of acid to the DMF solution. The neutral pyridylporphyrins are each reduced in two steps, located at $E_{1/2} = -0.99$ and -1.44 V for $\text{H}_2\text{Py}(\text{PhMe})_3\text{P}$ **1H₂**, and $E_{1/2} = -0.95$ and -1.36 V for $\text{H}_2\text{Py}_2(\text{PhMe})_2\text{P}$ **2H₂**. The stepwise shift in potential towards an easier reduction (as compared to H_2TPP) is expected, due to the larger electron-withdrawing properties of the pyridyl groups (as compared to a phenyl substituent).

Adding 5.0 eq TFA to the DMF solution containing $\text{H}_2\text{Py}(\text{PhMe})_3\text{P}$ **1H₂** or $\text{H}_2\text{Py}_2(\text{PhMe})_2\text{P}$ **2H₂** results in a shift towards more positive potentials, such that $\text{H}_2\text{Py}(\text{PhMe})_3\text{P}$ **1H₂** undergoes reductions at $E_p = -0.57$ and $E_p = -0.79$ V and $\text{H}_2\text{Py}_2(\text{PhMe})_2\text{P}$ **2H₂** exhibits reductions at $E_p = -0.38$ and $E_p = -0.60$ V, as shown in Figure 3-4b. All of the reductions are irreversible and a single reoxidation is seen at $E_p = -0.18$ and -0.04 V for the mono and dipyrrolylporphyrin, respectively.

The more facile reductions of $\text{H}_2\text{Py}(\text{PhMe})_3\text{P}$ **1H₂** and $\text{H}_2\text{Py}_2(\text{PhMe})_2\text{P}$ **2H₂** in DMF containing 5.0 eq TFA are consistent with the addition of protons to the pyridyl groups of the porphyrins, giving $[\text{H}_2\text{PyH}(\text{PhMe})_3\text{P}]^+$ and $[\text{H}_2(\text{PyH})_2(\text{PhMe})_2\text{P}]^{2+}$ as the

redox active species in solution. The peak potentials for the second reduction of the two porphyrins at -0.79 and -0.60 V are quite similar to $E_{1/2}$ values for the first reduction of the singly and doubly charged *N*-methylpyridyl porphyrins.¹⁸

The first reduction of the two compounds in Figure 3-4 at $E_p = -0.57$ and $E_p = -0.38$ V is associated with an irreversible electron addition to the fully protonated pyridylporphyrins having protonated core nitrogen atoms. The oxidations at -0.18 and -0.04 V are also assigned to processes involving compounds with protonated central nitrogens and this would then suggest a reduction and reoxidation mechanism such as the one shown in the third row (step iii) of Scheme 3-2, where the reduction involves electron addition to $[\text{H}_4\text{PyH}(\text{PhMe})_3\text{P}]^{3+}$ and $[\text{H}_4(\text{PyH})_2(\text{PhMe})_2\text{P}]^{4+}$, and the reoxidation involves electron abstraction from the same species.

There is no evidence for phlorin formation in DMF solutions with low TFA concentrations, but in the presence of excess TFA, the current-voltage curves resemble those described for H_2TPP and other related porphyrins. This is shown by the cyclic voltammograms in Figure 3-4c, where three redox processes are observed for each compound. The first corresponds to a two electron reduction of the fully protonated porphyrin at $E_{1/2} = -0.44$ V (for $[\text{H}_4\text{TPP}]^{2+}$), $E_{pc} = -0.22$ V (for $[\text{H}_4\text{PyH}(\text{PhMe})_3\text{P}]^{3+}$) and $E_{pc} = -0.09$ V (for $[\text{H}_4(\text{PyH})_2(\text{PhMe})_2\text{P}]^{4+}$). The electrogenerated dianion then reacts with excess acid in solution to give a phlorin anion which is reversibly reduced at $E_{1/2} = -0.67$, -0.60 or -0.51 V and irreversibly reoxidized at $E_{1/2} = 0.51$, 0.56 and 0.68 V, for the three compounds as shown in Figure 3-4c.

In each case, the shift of potential in a positive direction with an increase in the number of *meso*-pyridyl groups on the porphyrin is consistent with the known electron-withdrawing properties of the substituent. A summary of the above described mechanism is given in Scheme 3-2 for the **1H₂** and a similar mechanism is proposed for **2H₂**. The only difference is in the potential values for the indicated redox processes 1 to 7.

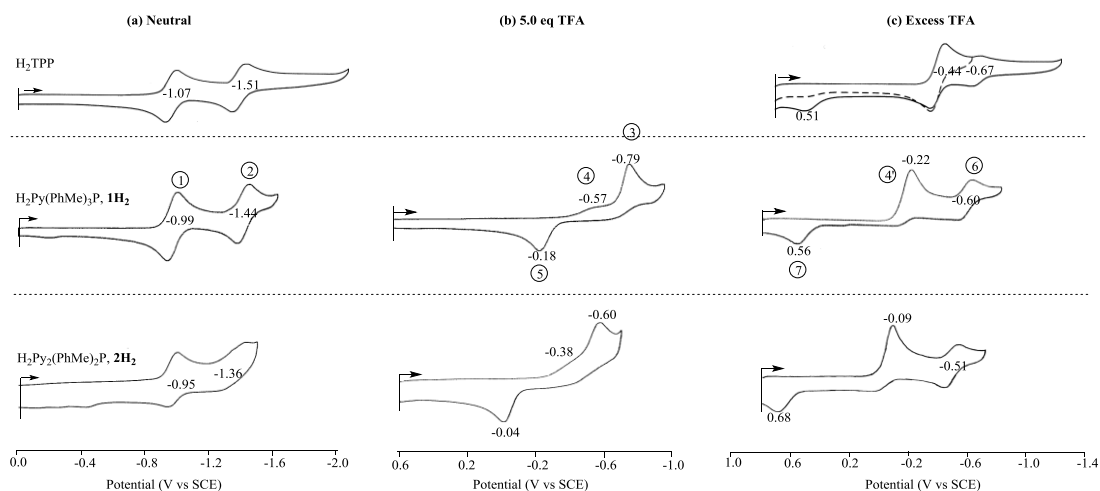
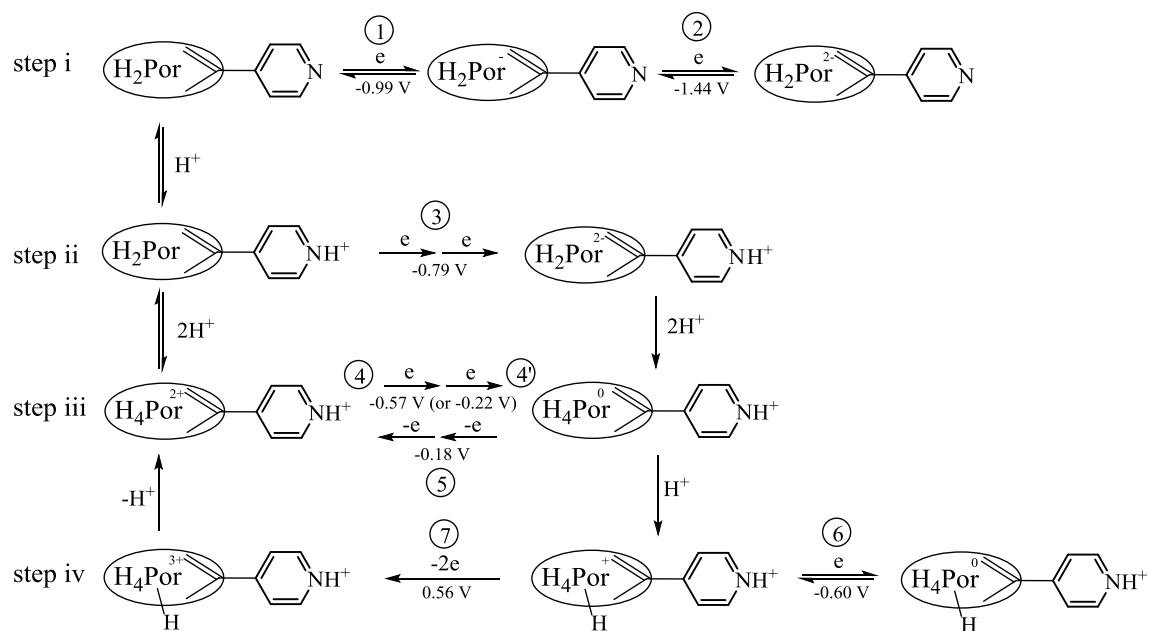


Figure 3-4. Cyclic voltammograms of H₂TPP, H₂Py(PhMe)₃P and H₂Py₂(PhMe)₂P ($\sim 10^{-4}$ M) in (a) DMF containing 0.1 M TBAP, (b) DMF containing 0.1 M TBAP and 5.0 eq TFA and (c) DMF containing excess TFA. The reactions occur for the processes labeled 1 to 7 are described in Scheme 3-2.

Scheme 3-2. Proposed reduction mechanism for $\text{H}_2\text{Py}(\text{PhMe})_3\text{P}$ before and after protonation in DMF. A similar mechanism is proposed for $\text{H}_2\text{Py}_2(\text{PhMe})_2\text{P}$ but with all potentials shifted positively, as shown by the cyclic voltammograms in Figure 3-4.



3.3 Conclusions

Acid-base and electrochemical properties of three free-base porphyrins with one, two or four *meso*-pyridyl substituent(s) were characterized in nonaqueous media. The protonation reactions of porphyrins in this series occurs in two steps: the first step involves the pyridyl substituent(s) and results in a systematic red shift in the position of the Soret band, as well as in the formation of a new Q band; the second protonation step involves the two core central nitrogen atoms of the porphyrin macrocycle. Protonation leads to a shift in the position of the Soret band and a new Q band. Protonation also has an effect on the electrochemical properties of this series of porphyrins which are easier to reduce as compared to the unprotonated parent compounds.

3.4 References

- (1) Cui, Y.; Zeng, L.; Fang, Y.; Zhu, J.; Xu, H.-J.; Desbois, N.; Gros, C. P.; Kadish, K. M. *ChemElectroChem* **2016**, *3*, 110.
- (2) Fang, Y.; Bhyrappa, P.; Ou, Z.; Kadish, K. M. *Chem. - Eur. J.* **2014**, *20*, 524.
- (3) Cui, Y.; Zeng, L.; Fang, Y.; Zhu, J.; Devillers, C. H.; Lucas, D.; Desbois, N.; Gros, C. P.; Kadish, K. M. *ChemElectroChem* **2016**, *3*(2), 228.
- (4) Ou, Z.; Shen, J.; Shao, J.; E, W.; Galezowski, M.; Gryko, D. T.; Kadish, K. M. *Inorg. Chem.* **2007**, *46*, 2775.
- (5) Daphnomili, D.; Landrou, G.; Prakash Singh, S.; Thomas, A.; Yesudas, K.; K, B.; Sharma, G. D.; Coutsolelos, A. G. *RSC Adv.* **2012**, *2*, 12899.
- (6) Engelmann, F. M.; Losco, P.; Winnischofer, H.; Araki, K.; Toma, H. E. *J. Porphyrins Phthalocyanines* **2002**, *6*, 33.
- (7) Dovidauskas, S.; Araki, K.; Toma, H. E. *J. Porphyrins Phthalocyanines* **2000**, *4*, 727.
- (8) Armaroli, N.; Diederich, F.; Echegoyen, L.; Habicher, T.; Flamigni, L.; Marconi, G.; Nierengarten, J.-F. *New Journal of Chemistry* **1999**, *23*, 77.
- (9) Araki, K.; Araujo, A. L.; Toyama, M. M.; Franco, M.; Azevedo, C. M. N.; Angnes, L.; Toma, H. E. *J. Porphyrins Phthalocyanines* **1998**, *2*, 467.
- (10) De Luca, G.; Romeo, A.; Scolaro, L. M. *J. Phys. Chem. B* **2005**, *109*, 7149.
- (11) Winnischofer, H.; Engelmann, F. M.; Toma, H. E.; Araki, K.; Rechenberg, H. R. *Inorg. Chim. Acta* **2002**, *338*, 27.
- (12) Kalyanasundaram, K. *Inorg. Chem.* **1984**, *23*, 2453.
- (13) Wang, C.; Wamser, C. C. *J. Phys. Chem. A* **2014**, *118*, 3605.
- (14) Wang, C.; Wamser, C. C. *J. Org. Chem.* **2015**, *80*, 7351.
- (15) Akins, D. L.; Zhu, H.-R.; Guo, C. *J. Phys. Chem.* **1996**, *100*, 5420.
- (16) De Luca, G.; Romeo, A.; Scolaro, L. M. *J. Phys. Chem. B* **2005**, *109*, 7149.
- (17) Wang, C.; Wamser, C. C. *J. Phys. Chem. A* **2014**, *118*, 3605.
- (18) Cui, Y., PhD. Dissertation, University of Houston, 2015.

Chapter Four

Electrochemistry and Acid-Base Properties of

Metallopyridylporphyrins in Nonaqueous Media

4.1 Introduction

Porphyrins and their analogues have attracted considerable attention for use in a broad range of applications.¹⁻¹⁷ Our own interest in porphyrins has been primarily in elucidating their solution redox properties as a function of changes in structures and solvent and, in this regard, our group recently reported the electrochemical reactions of free-base porphyrins in nonaqueous solvents.^{5,7-9}

In this chapter, we report how changes in the *meso*-substituents and overall charge of the porphyrin will affect the protonation, UV-vis spectra and electrochemistry of *meso*-pyridyl nitrogens for derivatives with different central metals. The structures of the investigated pyridylporphyrins are shown in Chart 4-1.

During the course of our studies we observed that changes in the UV-vis spectra during protonation of the cobalt pyridylporphyrins closely resembled spectral changes obtained upon electrooxidation of the compound in nonaqueous media.¹⁸⁻²⁴ This suggested to us that protonation of the porphyrin may result in a change of the initial Co(II) oxidation state of the compound, giving a Co(III) porphyrin product.

Co(II) porphyrins can exist as four, five or six-coordinate species while Co(III) porphyrins usually exist as five and six-coordinate species. The products of the pyridyl porphyrin protonation may aggregate due to a change in oxidation states of cobalt. The aggregation of porphyrin complexes in nonaqueous solvents is a well-known phenomenon² that affects both spectroscopic and electrochemical properties of these type complexes. To our knowledge, there have been no publications that reported similarities

between the products of protonation and the oxidation of the same metalloporphyrin in solution.

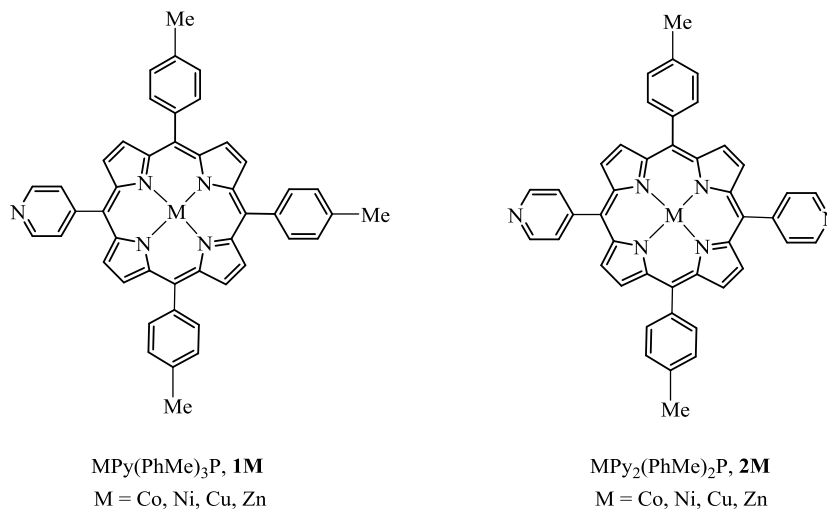


Chart 4-1. Structures of investigated metallopyridylporphyrins.

4.2 Results and Discussion

4.2.1 UV-vis Spectral Monitoring of Metallopyridylporphyrin Protonation

The UV-visible spectra of neutral NiPy(PhMe)₃Por, CuPy(PhMe)₃Por and ZnPy(PhMe)₃Por are virtually identical to each other in PhCN, each porphyrin being characterized by a sharp Soret band between 419 and 428 nm and a single Q band between 530 and 559 nm.

The spectral changes which occur upon titration with TFA for the mono-pyridyl metalloporphyrins **1M** where M = Cu, Ni and Zn are similar to the initial spectral changes observed for the free base porphyrins. These changes are described in Chapter 3 and are associated with protonation of the porphyrin pyridyl groups in the first step. The metallopyridylporphyrins can only be protonated on the *meso*-pyridyl group and when this occurs, the Soret band shifts by 3 nm in PhCN. The pyridyl protonation constant for **1Ni** and **1Cu** are 4.16 and 4.17, while logK = 4.50 for **1Zn** under the same solution conditions. For comparison, the measured pyridyl protonation constant of **1H₂** is logK = 3.79. Analysis of the spectral changes for the compounds in Chapter 3 confirmed that the initial protonation of the free-base pyridylporphyrins occurred at the pyridyl substituent(s) prior to protonation the central nitrogen atoms of the macrocycle.

The final UV-visible spectra of the fully protonated pyridylporphyrins are also similar to spectra of the mono-pyridyl metalloporphyrins **1M**, each spectrum being characterized by a decreased intensity Soret band located between 422 and 431 nm, as graphically shown in Figure 4.1.

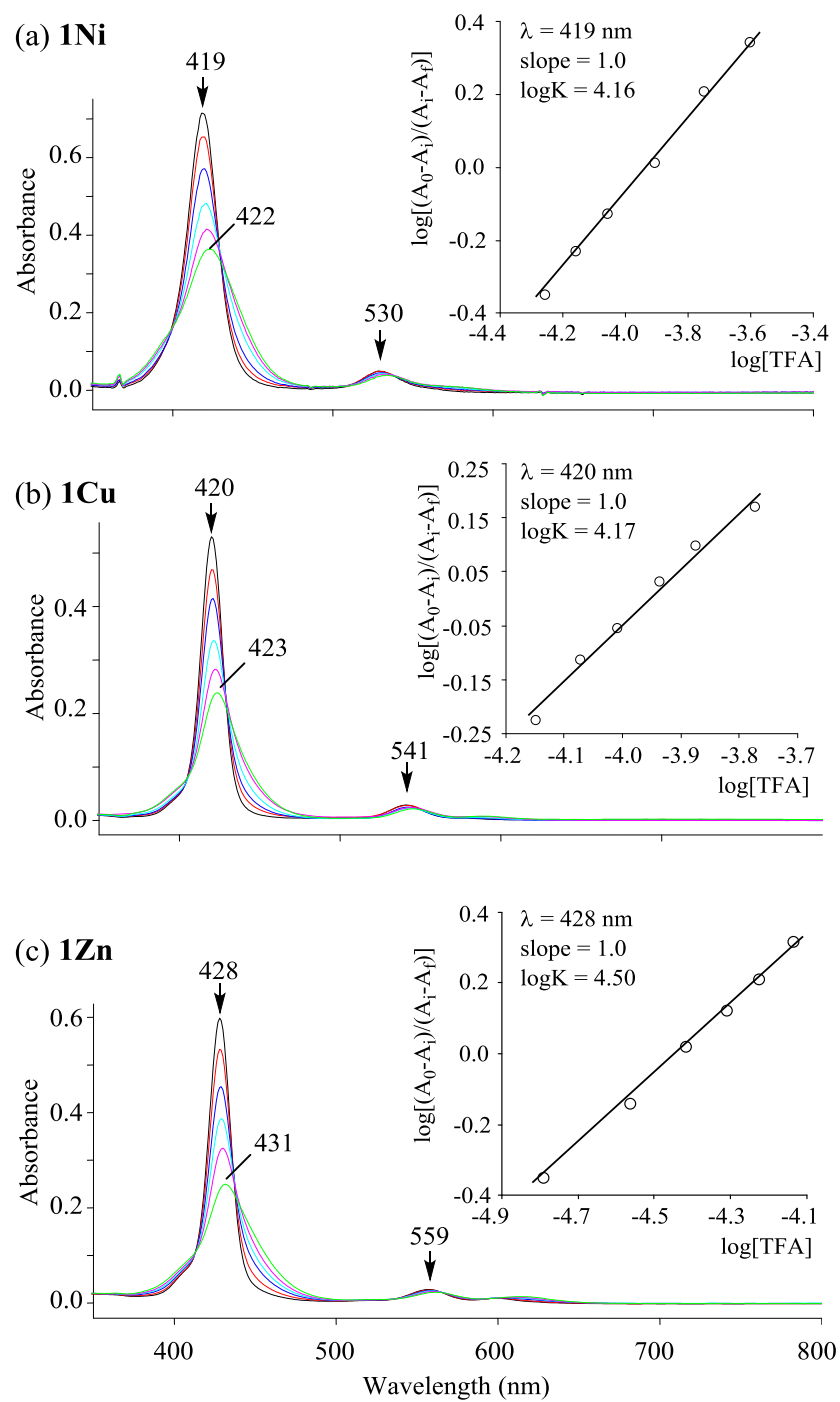


Figure 4-1. UV-visible spectral changes of **1Ni**, **1Cu** and **1Zn** in PhCN during titration with TFA. The figure insets show the Hill plots used for analysis.

4.2.2 Electrochemistry and Spectroelectrochemistry of Metallopyridylporphyrins

The electrochemistry of each metallopyridylporphyrins was characterized in PhCN, DMSO, DMF and CH₂Cl₂ containing 0.1 M TBAP. A summary of half-wave potentials for each reduction in these solvents is given in Table 4-1. Due to poor solubility, data could not be obtained for all of the compounds in each solvent.

Examples of cyclic voltammograms in PhCN containing 0.1 M TBAP are illustrated in Figure 4-2 for CuPy(PhMe)₃Por **1Cu**, NiPy(PhMe)₃Por **1Ni** and ZnPy(PhMe)₃Por **1Zn**. The electrochemical behavior of **1Cu**, **1Ni** and **1Zn** are similar to each other. In each case, there are two one-electron reductions located at half-wave potentials which are dependent upon the central metal in the macrocycle. **1Cu** has a first reversible reduction at $E_{1/2} = -1.32$ V and a second reversible reduction at $E_{1/2} = -1.69$ V. **1Ni** has a first reversible reduction at -1.23 V and a second reversible reduction at -1.62 V. **1Zn** has two reversible reductions at $E_{1/2} = -1.35$ and -1.74 V.

Electrochemical measurements of **1Co** and **2Co** could not be carried out in PhCN, CH₂Cl₂ or DMF due to low solubility, but well-defined current voltage curves were obtained in pyridine, as shown by the cyclic voltammogram in Figure 4-3 for **1Co**.

The two sets of non-coupled reduction and oxidation peaks in Figure 4-3 are related to changes in the degree of pyridine coordination by the porphyrin in its Co(II) and Co(III) oxidation states. This has been observed numerous times in the literature for a variety of related compounds where the initial Co(III) porphyrin in pyridine is 6-coordinate, the Co(II) porphyrin is 5-coordinate and the Co(I) porphyrin is 4-coordinate.

The “split” redox reactions at $E_{pc} = -0.42$ and $E_{pc} = 0.00$ V in Figure 4-3 and the associated oxidation/reduction mechanisms are associated in each case with an electrochemical EC mechanism, where the electron transfer step (E) is reversible and the chemical reaction following oxidation or reduction (C) involves the gain or loss of an axial ligand.^{1,22,23,25,26}

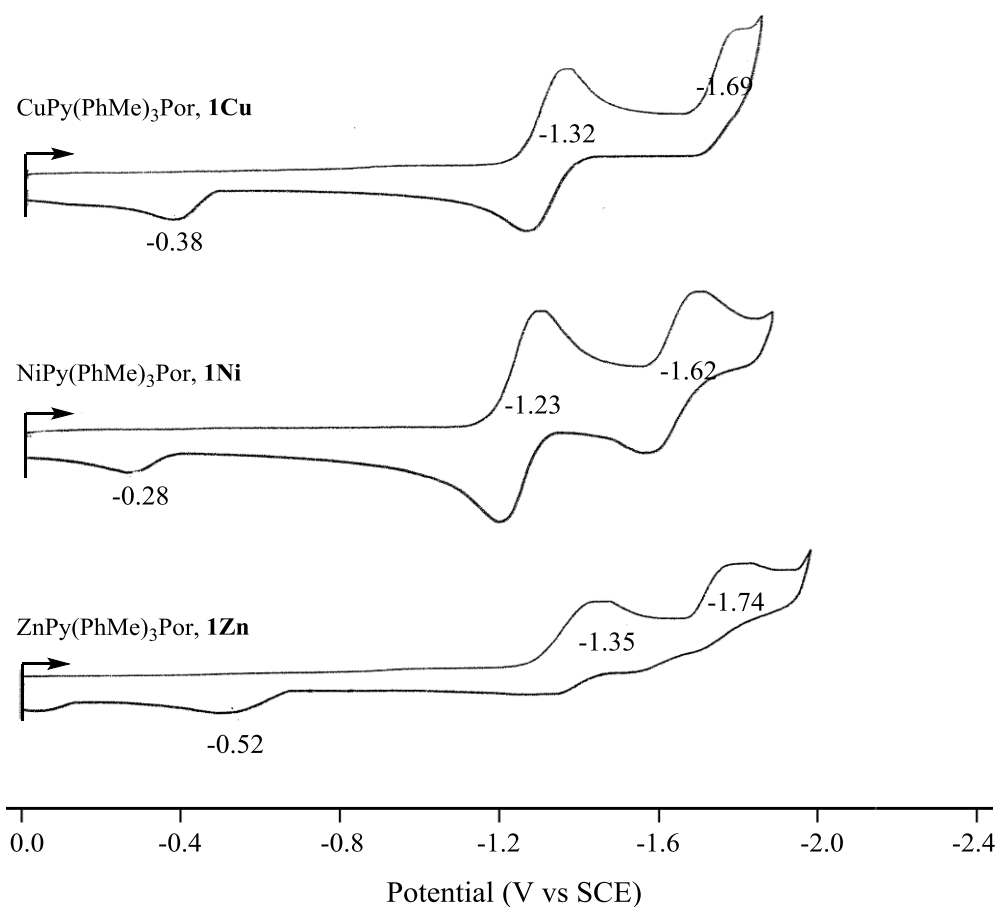


Figure 4-2. Cyclic voltammograms of CuPy(PhMe)₃Por (**1Cu**), NiPy(PhMe)₃Por (**1Ni**) and ZnPy(PhMe)₃Por (**1Zn**) in PhCN containing 0.1 M TBAP.

The first reduction of CoPy(PhMe)₃Por (**1Co**) in pyridine (abbreviated as pyrd) at $E_{pc} = -1.20$ V is coupled with a re-oxidation at $E_{pa} = -0.89$ V. The first oxidation of **1Co** in pyridine at $E_{pa} = 0.00$ V is coupled to a re-reduction at $E_{pc} = -0.42$ V. These reductions and oxidations all correspond to metal-centered reactions and the proposed mechanism for the Co^{II}/Co^{III} and Co^{II}/Co^I processes is given in Scheme 4-1. Only the metal center (Co^{III}, Co^{II} or Co^I) and the bound pyridine (pyrd) axial ligand are shown in the Scheme. This scheme is based in part on analysis of the current-voltage curves, in part on absorption spectra obtained during controlled potential electrolysis at 0.30 and -1.40 V in a thin layer spectroelectrochemical cell (Figure 4-3b) and in part on similar mechanisms proposed for a variety of structurally related cobalt porphyrins in pyridine.¹²

Table 4-1. Half-wave potentials (V vs SCE) of investigated mono- and di-pyridylporphyrins in different solvents containing 0.1 M TBAP. Scan rate = 0.1 V/s.

Solvent	M	Mono		Di	
		1 st red	2 nd red	1 st red	2 nd red
PhCN	2H	-1.12	-1.51	-1.06	-1.45
	Cu	-1.24	-1.69	-1.20	-1.64
	Ni	-1.23	-1.62	-1.18	-1.53
	Zn	-1.35	-1.74	a	a
DMSO	2H	-1.00	-1.42	-0.95 ^b	-1.36 ^b
	Cu	-1.15	-1.63	-1.09 ^b	-1.53 ^b
	Zn	-1.29 ^c	-1.69	-1.20 ^b	-1.64 ^b
DMF	2H	-0.99	-1.44	-1.00	-1.44
CH ₂ Cl ₂	2H	-1.18	-1.51	-1.14	-1.46
	Ni	-1.25	-1.58	-1.23	-1.53

^a Data could not be obtained due to the poor solubility of **2Zn**; ^bSecond scan;

^c An extra irreversible reduction was seen at $E_p = -0.84$ V

4.2.3 Aggregation of Zinc Pyridylporphyrin Before Addition of Acid

The UV-visible spectral changes recorded for **2Zn** in PhCN during titration with TFA are shown in Figure 4-4. The initial porphyrin has a Soret band at 428 nm and a Q band at 554 nm but as TFA is added to solution, the intensity of both bands decrease and the Soret band shifts to 431 nm. However, as more TFA is added to solution, the intensity of the band at 431, 560 and 619 nm all increase. This change can be accounted for by aggregation of the initial porphyrin and by a breaking up of the aggregate in the presence of higher acid concentrations, giving protonated **2Zn** in its monomeric form as a final product of the proton addition reaction.

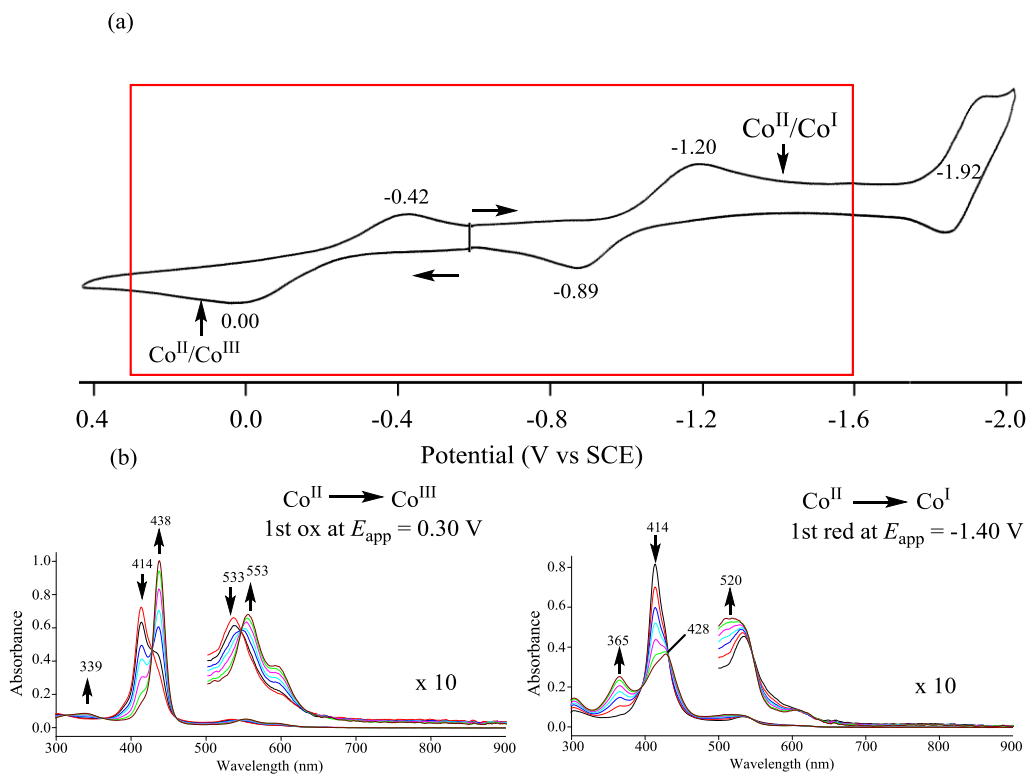


Figure 4-3. (a) Cyclic voltammograms and (b) UV-vis spectral changes for oxidation and reduction of CoPy(PhMe)₃Por **1Co** in pyridine.

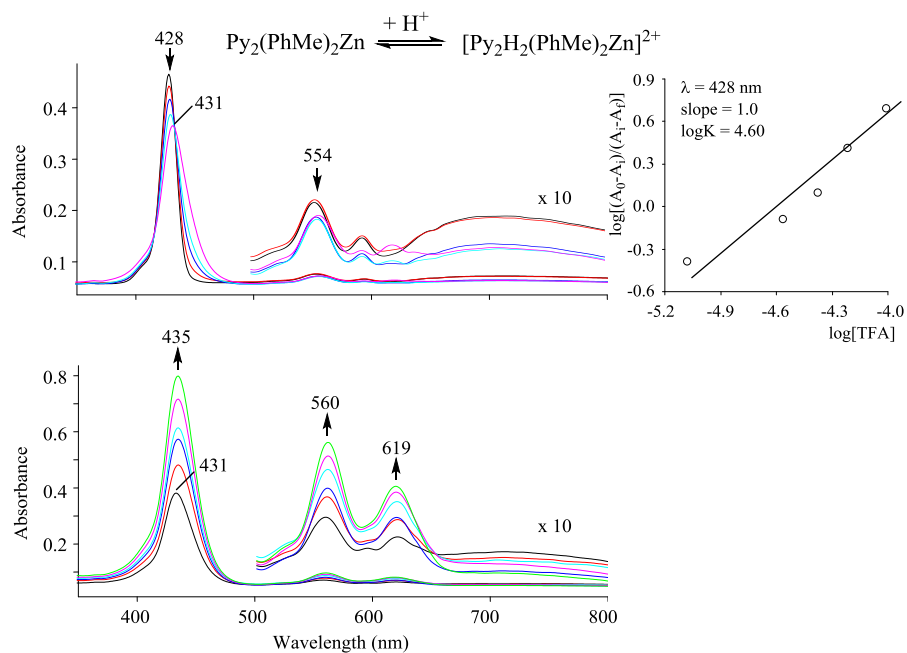
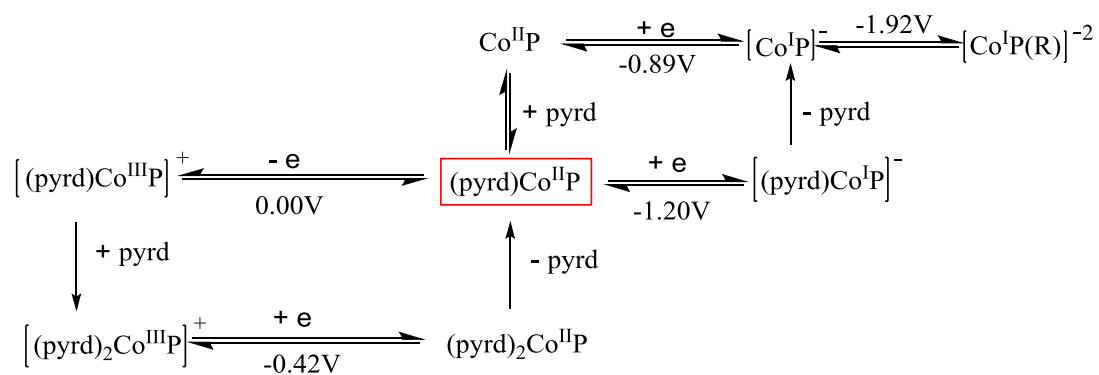


Figure 4-4. UV-visible spectra changes of **2Zn** in PhCN during titration with TFA. The figure inset shows the Hill plot used for analysis.

Scheme 4-1. Proposed mechanism for oxidation and reduction of $\text{Co}^{\text{II}}\text{Py}(\text{PhMe})_3\text{Por}$ **1Co** or $\text{Co}^{\text{II}}\text{Py}_2(\text{PhMe})_2\text{Por}$ **2Co** in pyridine, where P represents $\text{Py}(\text{PhMe})_3\text{Por}$ or $\text{Py}_2(\text{PhMe})_2\text{Por}$ and $\text{pyrd} = \text{pyridine}$. Only the central metal ion (Co^{III} , Co^{II} or Co^{I}) and axial ligand (pyrd) are shown). The initial 5-coordinate porphyrin in solutions of pyridine is shown in the red box.



4.2.4 Aggregation of Cobalt Pyridylporphyrin After Addition of Acid

Three types of UV-visible spectra are observed for CoPy(PhMe)₃Por (**1Co**) and CoPy₂(PhMe)₂Por (**2Co**) in pyridine. The first is for the Co(II) porphyrin which has bands at 414 and 533 nm and is 5-coordinate, as shown in Figure 4-4b and Scheme 4-1. The second is for the 6-coordinate Co(III) porphyrin which is characterized in pyridine by bands at 436-438 and 553-555 nm. Co(I) porphyrins do not bind axial ligands and the singly reduced 4-coordinate species is characterized by bands at 365, 428 and 520 nm, as shown by the spectroelectrochemical data in Figure 4-4b.

As discussed earlier in this thesis and shown in Figure 4-5, the one electron oxidation of **1Co** in pyridine leads to a species whose absorption spectrum is almost identical to that obtained upon addition of TFA to the same porphyrin in CH₂Cl₂. One equivalent of protons is needed to generate the Co(III) spectrum shown in Figure 4-5b and this can be accounted for by the initial formation of a mono-protonated pyridylporphyrin followed by a rapid internal transfer of an electron and oxidation of the Co(II) center, as illustrated in Scheme 4-2.

The chemically generated Co(III) porphyrin formed in Step 1 of Scheme 4-2 will then rapidly self-associate via axial coordination of a pyridyl group from one molecule to the central cobalt ion of another. The identity of the final product in this reaction is unknown but it must involve a higher aggregated form of the Co(III) porphyrin, an example of which is shown in the Scheme 4-2.

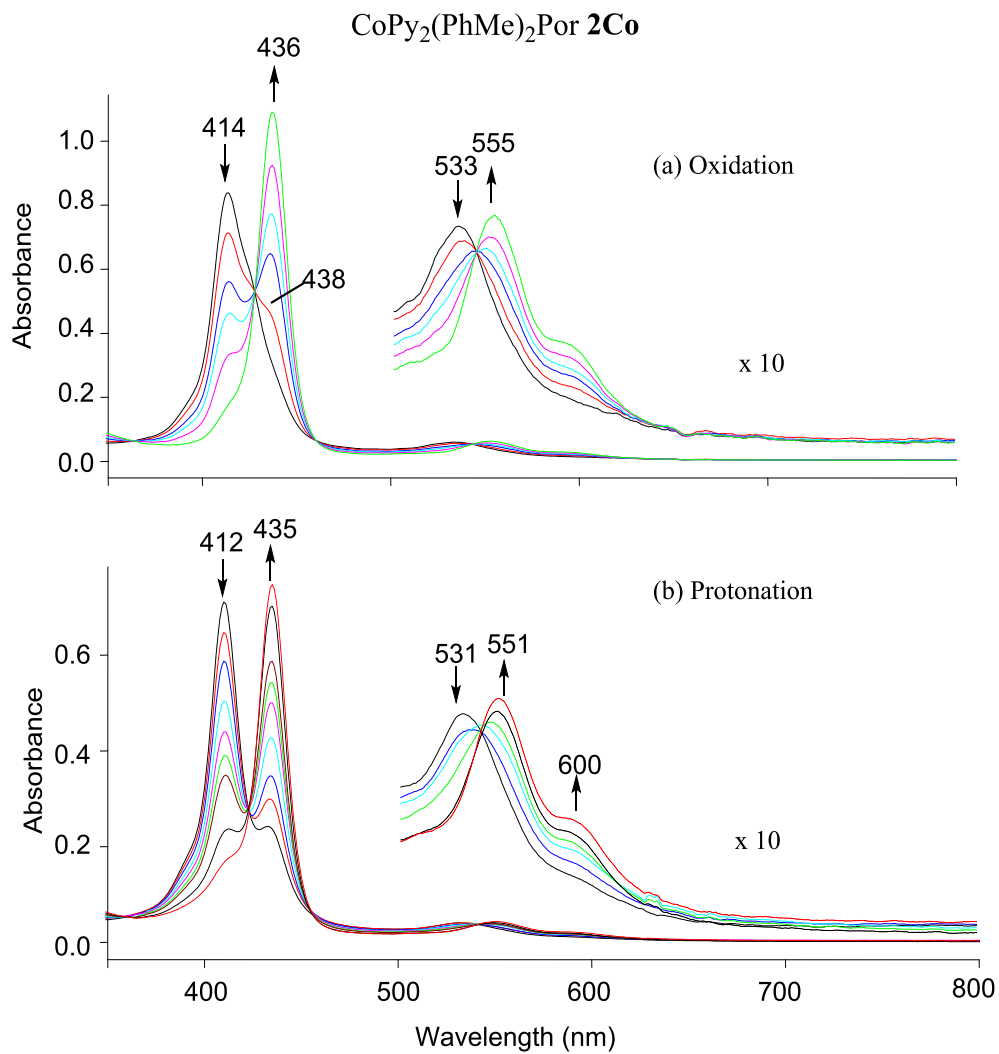
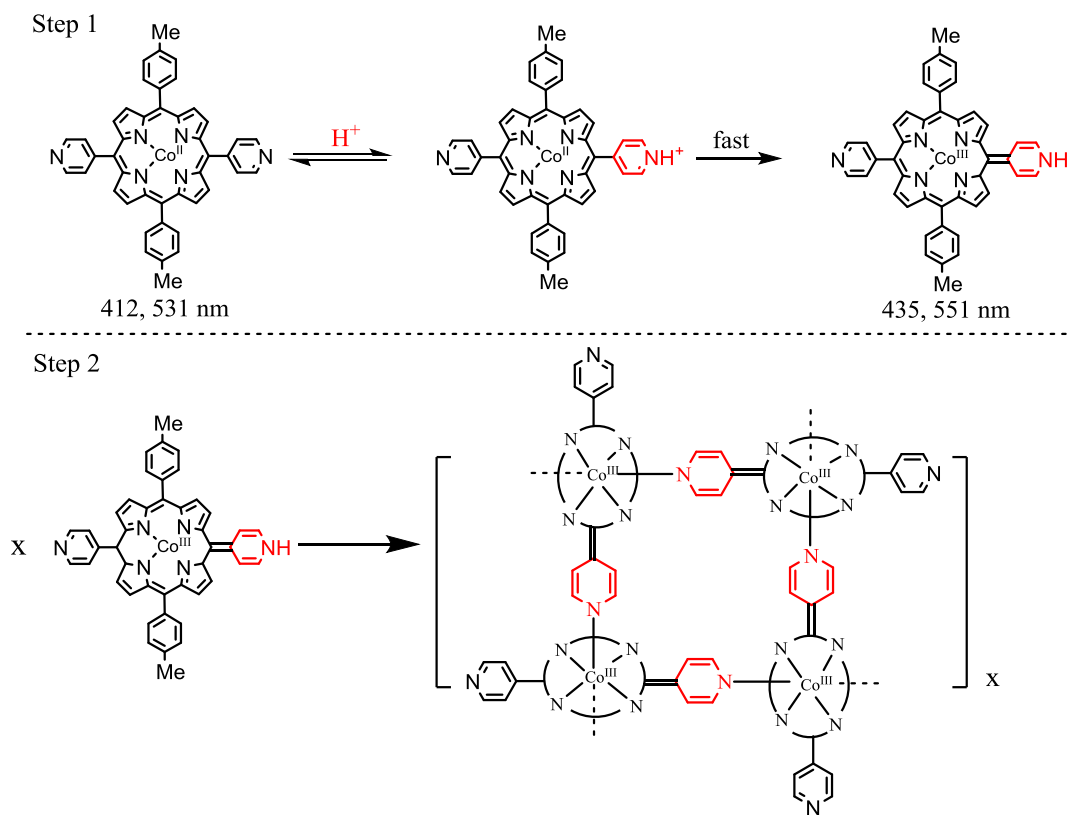


Figure 4-5. Spectral changes of CoPy₂(PhMe)₂Por **2Co** (a) upon a one electron oxidation at 0.30V in pyridine and (b) during the first protonation step of the neutral porphyrin in CH₂Cl₂.

Scheme 4-2. Proposed protonation and aggregation of oxidized CoPy₂(PhMe)₂Por **1Co**.



4.3 Conclusions

In this chapter we report the electrochemistry and acid-base properties of metallopyridylporphyrins of the form $\text{MPy}_x(\text{PhMe})_{4-x}\text{P}$, where $\text{M} = \text{Co(II)}, \text{Ni(II)}, \text{Cu(II)}$ or Zn(II) . This series of complexes is easily protonated on the *meso*-pyridyl substituents. The Cu(II) , Ni(II) and Zn(II) pyridylporphyrins exhibit similar reduction behavior; each porphyrin undergoes two reversible reductions. The UV-vis data suggest that **2Zn** is aggregated before the addition of protons but that monomers are formed after the addition of protons to solution; in contrast, the Co(II) pyridylporphyrins are converted to their Co(III) form after protonation and aggregation then occurs.

4.4 References

- (1) Kadish, K. M.; Smith, K. M.; Guillard, R. *Handbook of Porphyrin Science*; World Scientific: Singapore, 2010-2014; Vol. 1-35.
- (2) Kadish, K. M.; Smith, K. M.; Guillard, R. *The Porphyrin Handbook*; Academic Press: New York, 2000-2003; Vol. 1-20.
- (3) Li, W.; Zhang, Q.; Zhou, H.; Chen, J.; Li, Y.; Zhang, C.; Yu, C. *Anal. Chem. (Washington, DC, U. S.)* **2015**, *87*, 8336.
- (4) Jacobsen, J. L.; Berget, P. E.; Varela, M. C.; Vu, T.; Schore, N. E.; Martin, K. E.; Shelnut, J. A.; Santos, L. M.; Medforth, C. J. *Tetrahedron* **2013**, *69*, 10507.
- (5) Keane, P. M.; Kelly, J. M. *Photochem. Photobiol. Sci.* **2011**, *10*, 1578.
- (6) Hargrove, A. E.; Nieto, S.; Zhang, T.; Sessler, J. L.; Anslyn, E. V. *Chem. Rev. (Washington, DC, U. S.)* **2011**, *111*, 6603.
- (7) Fang, Y.; Bhyrappa, P.; Ou, Z.; Kadish, K. M. *Chem. - Eur. J.* **2014**, *20*, 524.
- (8) Cui, Y.; Zeng, L.; Fang, Y.; Zhu, J.; Xu, H.-J.; Desbois, N.; Gros, C. P.; Kadish, K. M. *ChemElectroChem* **2016**, *3*, 110.
- (9) Cui, Y.; Zeng, L.; Fang, Y.; Zhu, J.; Devillers, C. H.; Lucas, D.; Desbois, N.; Gros, C. P.; Kadish, K. M. *ChemElectroChem* **2016**, *3* (2), 228.
- (10) Heiling, G.; Wilson, G. *Anal. Chem.* **1971**, *43*, 545.
- (11) Su, B.; Li, F.; Nia, R.; Gros, C.; Barbe, J.; Samec, Z.; Girault, H. *Chem. Commun.* **2008**, 5037.
- (12) Thyagarajan, S.; Leiding, T.; Arskold, S. P.; Cheprakov, A. V.; Vinogradov, S. A. *Inorg. Chem.* **2010**, *49*, 9909.
- (13) Rosa, A.; Ricciardi, G.; Baerends, E.; Romeo, A.; Scolaro, L. *J. Phys. Chem. A* **2003**, *107*, 11468.
- (14) Wang, C.; Wamser, C. C. *J. Phys. Chem. A* **2014**, *118*, 3605.
- (15) Winnischofer, H.; Engelmann, F. M.; Toma, H. E.; Araki, K.; Rechenberg, H. R. *Inorg. Chim. Acta* **2002**, *338*, 27.
- (16) Wang, C.; Wamser, C. C. *J. Org. Chem.* **2015**, *80*, 7351.
- (17) De Luca, G.; Romeo, A.; Scolaro, L. M. *J. Phys. Chem. B* **2005**, *109*, 7149.
- (18) Araullo-McAdams, C.; Kadish, K. M. *Inorg. Chem.* **1990**, *29*, 2749.
- (19) D'Souza, F.; Villard, A.; Van Caemelbecke, E.; Franzen, M.; Boschi, T.; Tagliatesta, P.; Kadish, K. M. *Inorg. Chem.* **1993**, *32*, 4042.
- (20) Kadish, K. M.; Lin, X. Q.; Han, B. C. *Inorg. Chem.* **1987**, *26*, 4161.
- (21) Lin, X. Q.; Boisselier-Cocolios, B.; Kadish, K. M. *Inorg. Chem.* **1986**, *25*, 3242.
- (22) Truxillo, L. A.; Davis, D. G. *Anal. Chem.* **1975**, *47*, 2260.
- (23) Wolberg, A. *Isr. J. Chem.* **1974**, *12*, 1031.
- (24) Wolberg, A.; Manassen, J. *J. Amer. Chem. Soc.* **1970**, *92*, 2982.
- (25) Scholz, W. F.; Reed, C. A.; Lee, Y. J.; Scheidt, W. R.; Lang, G. *J. Am. Chem. Soc.* **1982**, *104*, 6791.

(26) Salehi, A.; Oertling, W. A.; Babcock, G. T.; Chang, C. K. *J. Am. Chem. Soc.* **1986**, *108*, 5630.

Chapter Five

Electrochemical Studies of

Free-base Tetra-*N*-methylpyridylporphyrins

5.1 Introduction

In the early 1970s, the first examples of synthetic water-soluble porphyrins were reported.¹ These compounds contained four negatively charged *meso*-substituents (i.e. tetra-4-sulfonatophenylporphyrin TPPS) or four positively charged substituents at the *meso* positions of the macrocycle (i.e., tetra-4-*N*-methylpyridinium porphyrin TMPyP)². A few years later, the therapeutic potential of Fe^{III} TMPyP was mentioned by Pasternack and Halliwell, who showed that compound catalyzed the conversion of superoxide to give H₂O₂ and O₂.³ Due to their great stability, biocompatibility and ability to generate reactive oxygen species as well as the possibility to modify their structure and properties, water-soluble porphyrins were rapidly found to be promising candidates for many biological and medical applications.⁴ From then on, numerous other charged⁵ or neutral⁶ water-soluble porphyrins have been synthesized. Despite the synthesis of many related important derivatives, the interest in TMPyP has remained high over the years.

In 1972, Pasternack showed that, unlike anionic porphyrins such as TPPS, the cationic TMPyP tends to aggregate less than anionic TPPS in water at concentration of $>10^{-4}$ M.⁷ Pasternack explained this result by a delocalization of the positive charges of the pyridinium groups onto the porphyrin ring that leads to a Coulombic repulsion between the molecules. The monomeric character of TMPyP at concentrations below $<10^{-3}$ M was later confirmed by Kano,⁸ who compared its NMR spectrum with that of dimers formed by *cis*- and *trans*- 4-*N*-methylpyridiniumporphyrins.

The aggregation properties of a given positively or negatively charged molecule are also strongly affected by the nature of any associated counterions, since changes in

the counterion can lead to significant changes in solubility. Charged compounds with small counterions tend to be less soluble than compounds with large counterions. This is because small ions bond more closely together than large ions, and they are harder to break apart, making them less soluble. Recently, the role of counteranions in the acid-induced aggregation of tetrapyridylporphyrins in organic solvents was reported by De Luca et. al.⁹ The protonated species and resulting aggregates exhibit UV-visible spectra, which are significantly influenced by the nature of the counteranions.⁹ Moreover, depending on the type of anions, the porphyrin chromophores adopt different spatial arrangements that lead to a large variety of aggregates.

Hurley and coworkers discovered a key property of the cationic TMPyP: this derivative is able to selectively stack as G-tetrads that stabilize quadruplex DNA, resulting in the inhibition of the telomerase.¹⁰ In 2014, Jiang and coworkers studied the influence of two counterions, chloride and tosylate, on the binding properties of the TMPyP with G-quadruplex.¹¹ Based on UV-melting measurements, molecular modeling and mass spectrometry experiments, they concluded that tosylate contributes to the stabilizing effect of TMPyP tetratosylate on the DNA G-quadruplex.¹¹ Furthermore, due to its photophysical properties, together with its monomeric character in aqueous media, TMPyP acts as an efficient photosensitizer to produce singlet oxygen. With this in mind, the derivative was further explored as a therapeutic, anti-angiogenic and antimicrobial drug.⁴ Despite the obvious interest of this porphyrin, few investigations have focused on the role of anions in the electrochemistry of these compounds and the literature lacks data about the influence on the physicochemical properties of these molecules. Nevertheless,

several strategies were developed to easily change the nature of the counteranions.^{12,13} This adjustability is advantageous for fine-tuning the physical and chemical properties of the molecule.

In the current chapter, we describe spectroscopic and electrochemical measurements carried out on a series tetra-*N*-methylpyridylporphyrins (shown in Chart 5-1) with different counteranions in DMF and DMSO containing TBAPF₆ or TBAI as supporting electrolyte. The examined compounds were synthesized in Dijon, France by our collaborator Dr. Roger Guillard, in collaboration with PorphyChem.

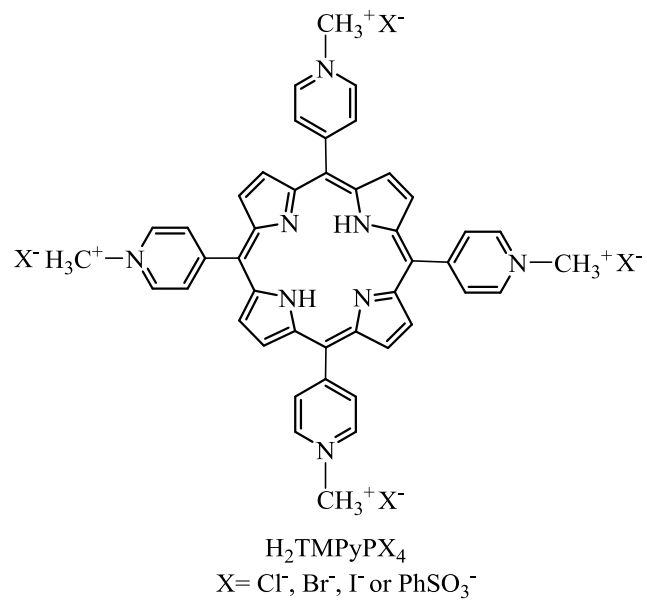


Chart 5-1. Molecular structures of the investigated porphyrins.

5.2 Results and Discussion

5.2.1 Electrochemistry

Figures 5-1 and 5-2 illustrate cyclic voltammograms of the metal-free $[\text{H}_2\text{TMPyP}]^{4+}(\text{X}^-)_4$ where $\text{X} = \text{Cl}^-$, Br^- , I^- or PhSO_3^- in DMSO or DMF, containing 0.1 M TBAPF_6 or TBAI. UV-vis data in of the compounds under these solution conditions are summarized in Table 5-1.

As shown in Figure 5-1, this series of compounds all exhibit six reversible reductions in DMSO, containing 0.1 M TBAPF_6 or TBAI, with half-wave potentials ranging from -0.47 to -1.11 V. However, when the solvent was changed to DMF, several of the reductions became overlapped, as shown in Figure 5-2. Half-wave potentials for reductions in both solvents with different electrolytes are summarized in Table 5-1.

In contrast to the free-base derivatives, the metalated tetra-*N*-methylpyridylporphyrins $[\text{TMPyPM}]^{4+}$, where $\text{M} = \text{Cu}(\text{II})$, $\text{Zn}(\text{II})$ or $\text{VO}(\text{II})$, exhibit three two-electron reductions in DMF.^{14,15} The first reduction was assigned as involving electron addition to the porphyrin macrocycle, while the later two were assigned as involving reductions of the four external pyridiniums.

The number of redox processes and potentials for reduction of $[\text{H}_2\text{TMPyP}]^{4+}(\text{X}^-)_4$ in DMSO and DMF vary greatly with change of the solvent, counteranion on the compound and type of utilized supporting electrolyte. This can be seen by the cyclic voltammograms in Figures 5-1 and 5-2. The use of DMSO as a solvent, 0.1 M TBAI as supporting electrolyte and PhSO_3^- as the counteranion gives the best defined processes among the different investigated conditions.

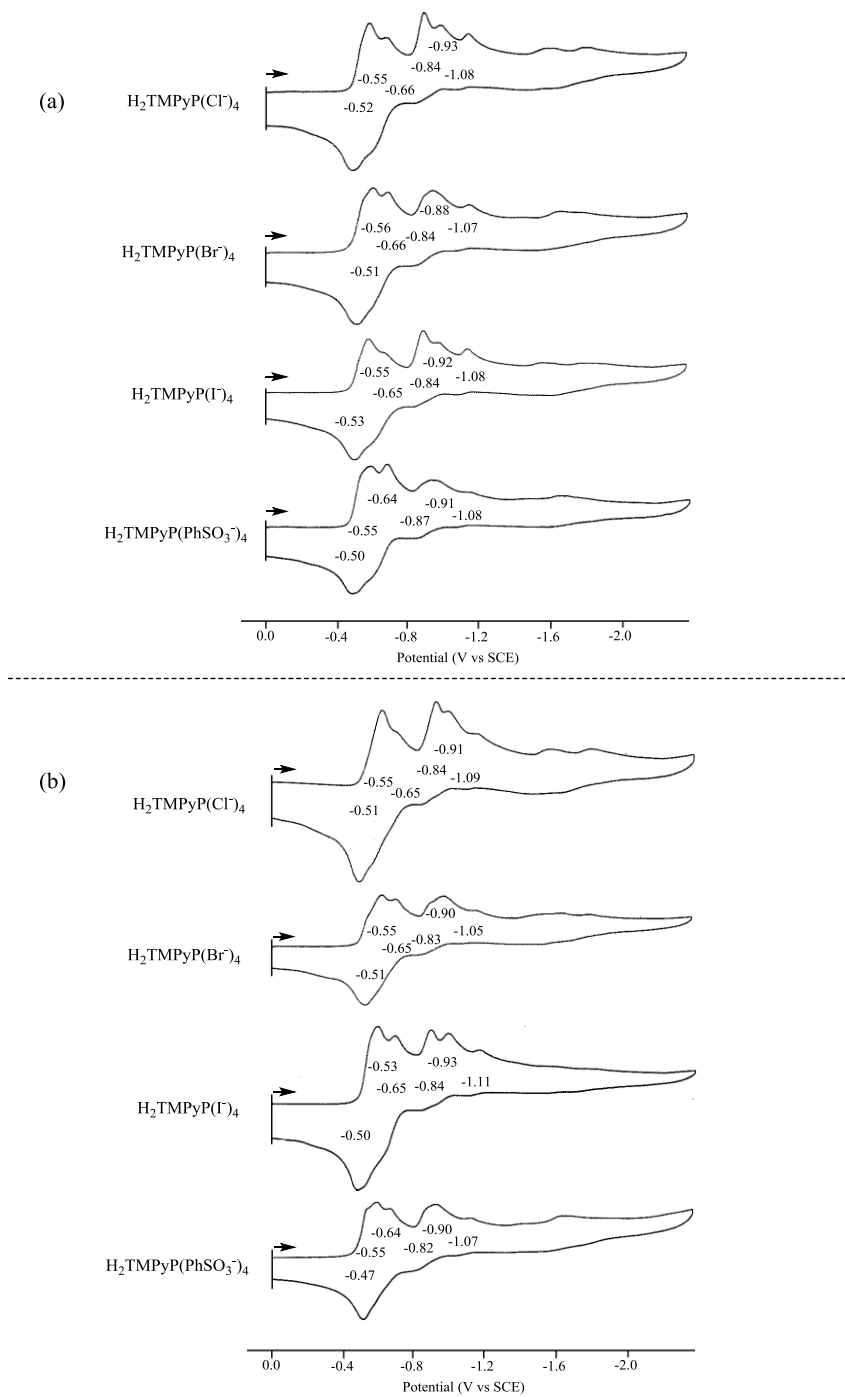


Figure 5-1. Cyclic voltammograms of $[H_2TMPyP]^{4+}(X^-)_4$ in DMSO containing 0.1 M (a) TBAPF₆ and (b) TBAI. Scan rate = 0.1 V/s.

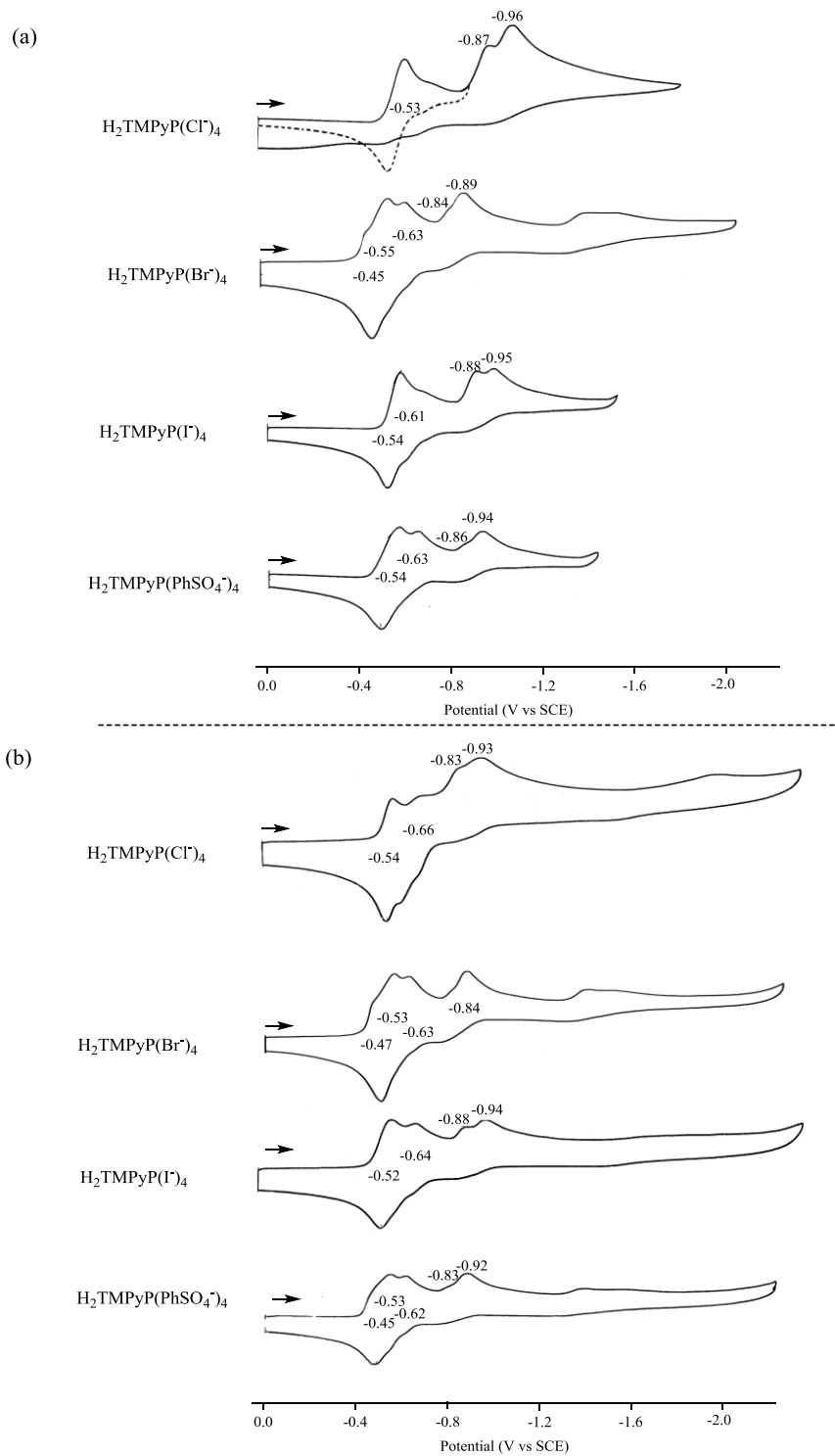


Figure 5-2. Cyclic voltammograms of $[\text{H}_2\text{TMPyP}]^{4+}(\text{X}^-)_4$ in DMF containing 0.1 M (a) TBAPF_6 or (b) TBAI. Scan rate = 0.1V/s.

5.2.2 UV-Vis Spectroscopy

Spectroscopic data for the tetra-*N*-methylpyridylporphyrins with different counteranions are summarized in Table 5-2. As seen in the table, the UV-vis spectra of the initial compounds are similar to each other, which means that neither the solvent, counteranion or supporting electrolyte has an effect on UV-vis spectroscopic properties of the initial compound in the two investigated solvents.

Table 5-1. Half-wave reduction potentials of TMPyPX₄ in DMSO or DMF containing 0.1M TBAI or 0.1M TBAPF₆.

solvent	electrolyte	anion	1 st red	2 nd red	3 rd red	4 th red	5 th red	6 th red	
DMF	TBAPF ₆	Cl ⁻	-0.53	-0.87 ^a	-0.96 ^a				
		Br ⁻	-0.45	-0.55	-0.63	-0.84 ^a	-0.89 ^a	-1.42 ^a	
		I ⁻	-0.54	-0.61	-0.88 ^a	-0.95 ^a			
		PhSO ₄ ⁻	-0.54	-0.63	-0.86 ^a	-0.94 ^a			
	TBAI	Cl ⁻	-0.54	-0.66	-0.83 ^a	-0.93 ^a	-1.90 ^a		
		Br ⁻	-0.47	-0.53	-0.63	-0.84	-1.40 ^a		
		I ⁻	-0.52	-0.64	-0.88 ^a	-0.94 ^a			
		PhSO ₄ ⁻	-0.45	-0.53	-0.62	-0.83 ^a	-0.92 ^a	-1.44 ^a	
DMSO	TBAPF ₆	Cl ⁻	-0.52	-0.55	-0.66	-0.84	-0.93	-1.08	
		Br ⁻	-0.51	-0.56	-0.66	-0.84	-0.88	-1.07	
		I ⁻	-0.53	-0.55	-0.65	-0.84	-0.92	-1.08	
		PhSO ₄ ⁻	-0.50	-0.55	-0.64	-0.87	-0.91	-1.08	
	TBAI	Cl ⁻	-0.51	-0.55	-0.65	-0.84	-0.91	-1.09	
		Br ⁻	-0.51	-0.55	-0.65	-0.83	-0.90	-1.05	
		I ⁻	-0.50	-0.53	-0.65	-0.84	-0.93	-1.11	
		PhSO ₄ ⁻	-0.47	-0.55	-0.64	-0.82	-0.90	-1.07	

^a irreversible reduction

Table 5-2. UV-vis data of $[\text{H}_2\text{TMPyP}]^{4+}(\text{X}^-)_4$ in DMSO or DMF containing 0.1M TBAI or 0.1M TBAPF₆.

solvent	electrolyte	compound	λ_{max} (nm)					electrolyte	Por	λ_{max}				
			Soret	Q bands						Soret	Q bands			
DMSO	TBAI	H ₂ TMPyPCL ₄	425	517	551	588	644	TBAPF ₆	H ₂ TMPyPCL ₄	424	516	554	590	643
		H ₂ TMPyPBr ₄	425	516	553	586	644		H ₂ TMPyPBr ₄	424	516	553	589	644
		H ₂ TMPyPI ₄	425	516	555	588	643		H ₂ TMPyPI ₄	424	517	554	588	642
		H ₂ TMPyP(PhSO ₃) ₄	424	518	553	589	644		H ₂ TMPyP(PhSO ₃) ₄	424	517	551	591	643
DMF	TBAI	H ₂ TMPyPCL ₄	425	520	558	592	646	TBAPF ₆	H ₂ TMPyPCL ₄	425	517	556	590	650
		H ₂ TMPyPBr ₄	424	518	554	592	648		H ₂ TMPyPBr ₄	424	516	555	590	651
		H ₂ TMPyPI ₄	425	517	553	593	651		H ₂ TMPyPI ₄	425	518	552	591	647
		H ₂ TMPyP(PhSO ₃) ₄	424	516	553	592	651		H ₂ TMPyP(PhSO ₃) ₄	424	516	552	591	650

5.3 Conclusions

Four tetra-*N*-methylpyridylporphyrins with different counteranions were characterized by UV-vis spectroscopy and electrochemistry in DMSO and DMF, containing 0.1 M TBAPF₆ or TBAI. The exact number of reductions and their reversibility are influenced by the type of solvent, the supporting electrolyte and/or the counteranion on the compound. Each porphyrin undergoes between three and six reductions at potentials between -0.45 to -1.11 V vs. SCE.

5.4 References

- (1) Fleischer, E. B.; Palmer, J. M.; Srivastava, T. S.; Chatterjee, A. *J Am Chem Soc* **1971**, *93*, 3162.
- (2) Hambright, P.; Fleischer, E. B. *Inorg. Chem.* **1970**, *9*, 1757.
- (3) Pasternack, R. F.; Halliwell, B. *J. Am. Chem. Soc.* **1979**, *101*, 1026.
- (4) Kadish, K. M.; Smith, K. M.; Guillard, R. *Handbook of Porphyrin Science*; World Scientific: Singapore, 2010-2014; Vol. 8.
- (5) Kadish, K. M.; Smith, K. M.; Guillard, R. *The Porphyrin Handbook*; Academic Press: New York, 2000-2003; Vol. 1-20.
- (6) Karunakaran, S. C.; Babu, P. S. S.; Madhuri, B.; Marydasan, B.; Paul, A. K.; Nair, A. S.; Rao, K. S.; Srinivasan, A.; Chandrashekar, T. K.; Rao, C. M.; Pillai, R.; Ramaiah, D. *ACS Chem. Biol.* **2013**, *8*, 127.
- (7) Pasternack, R. F.; Huber, P. R.; Boyd, P.; Engasser, G.; Francesconi, L.; Gibbs, E.; Fasella, P.; Cerio Venturo, G.; Hinds, L. d. *J. Amer. Chem. Soc.* **1972**, *94*, 4511.
- (8) Kano, K.; Minamizono, H.; Kitae, T.; Negi, S. *J. Phys. Chem. A* **1997**, *101*, 6118.
- (9) De Luca, G.; Romeo, A.; Scolaro, L. M. *J. Phys. Chem. B* **2005**, *109*, 7149.
- (10) Wheelhouse, R. T.; Sun, D.; Han, H.; Han, F. X.; Hurley, L. H. *J. Am. Chem. Soc.* **1998**, *120*, 3261.
- (11) Bai, L.-P.; Liu, J.; Han, L.; Ho, H.-M.; Wang, R.; Jiang, Z.-H. *Anal. Bioanal. Chem.* **2014**, *406*, 5455.
- (12) Gong, X.; Milic, T.; Xu, C.; Batteas, J. D.; Drain, C. M. *J. Am. Chem. Soc.* **2002**, *124*, 14290.
- (13) Yao, H.; Sasahara, H.; Kimura, K. *Chem. Mater.* **2011**, *23*, 913.
- (14) Van Caemelbecke, E.; Derbin, A.; Hambright, P.; Garcia, R.; Doukkali, A.; Saoiabi, A.; Ohkubo, K.; Fukuzumi, S.; Kadish, K. M. *Inorg. Chem.* **2005**, *44*, 3789.
- (15) Kadish, K. M.; Araullo, C.; Maiya, G. B.; Sazou, D.; Barbe, J. M.; Guillard, R. *Inorg. Chem.* **1989**, *28*, 2528.

Chapter Six

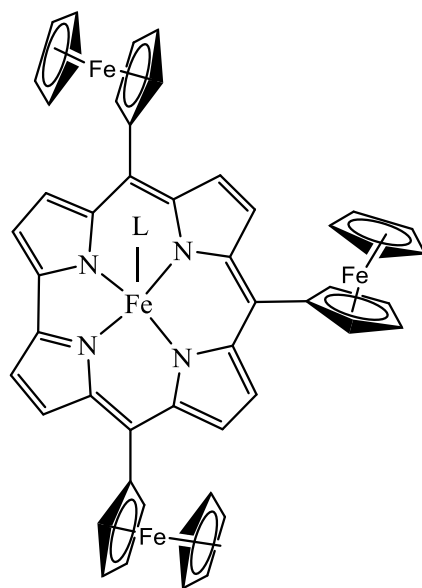
Electrochemical Studies of Ferrocenylcorrole Complexes

6.1 Introduction

Porphyryns¹⁻¹⁰ and porphyrinoids, such as phthalocyanines,^{11,12} tetraazaporphyrins¹³⁻¹⁵ and corroles¹⁶⁻¹⁹ with linked ferrocene substituents are of interest due to their importance in the development of molecular-based electronic devices²⁰⁻²³ and molecular electrogenic sensors.²⁴ These types of compounds can accept and/or release multiple electrons and are important in the area of multielectron redox catalysis²⁵ and information storage at the molecular level.^{26,27}

Iron corroles containing ferrocene groups at the three *meso*-positions of the corrole macrocycle have been shown to undergo oxidations at the Fc units and have been studied as “mixed-valence state” derivatives.^{28,29} Corroles act as trianionic ligands, which are characterized by facile oxidations and the ability to induce facile ligand-to-metal electron transfers. Adding electron-donor ferrocenyl substituents at the *meso*-positions of the corrole macrocycle will enhance the tendency of these compounds to undergo an oxidation process.

A series of iron 5,10,15-triferrocenylcorroles ligands were prepared by our collaborators in Rome and sent to us for investigation of their electrochemical properties. The structures of these compounds are shown in Chart 6-1. As shown in the chart, the difference in this series of compounds is both in the type of axial ligand bound to the central metal ion and the formal oxidation state of the iron in the initial form of the corrole. We wished to investigate how the different axial ligands on the central iron would influence the electrochemical properties of these compounds and we also wished to investigate the redox properties of the three linked Fc units.



L = NO, Ph or Cl

Chart 6-1. Molecular structures of investigated Fe corroles.

6.2 Results and Discussion

6.2.1 Electrochemistry of Iron Ferrocenecorrole

Cyclic voltammograms of the investigated corroles in PhCN containing 0.05 M tetrakis-fluorophenyl borate(TFAB) as supporting electrolyte are shown in Figure 6-1. This series of corroles exhibits three reversible one-electron oxidations of the linked ferrocene groups at $E_{1/2}$ values ranging from 0.50 to 0.79 V. Each ferrocenylcorrole also undergoes one or two reductions at $E_{1/2}$ values of -1.76 to -1.95 V.

As seen in Figure 6-1, the formal $\text{Fe}^{\text{III}}/\text{Fe}^{\text{II}}$ reaction of $\text{TFcCorrFe}^{\text{III}}(\text{NO})$ and the formal $\text{Fe}^{\text{IV}}/\text{Fe}^{\text{III}}$ reaction of $\text{TFcCorrFe}^{\text{IV}}(\text{C}_6\text{H}_5)$ are located at identical half wave potentials of -0.43 V vs SCE. A second reduction of the two compounds is located at -1.83 and -1.76 V, respectively.

Reduction of the iron corroles can occur at the iron center, at the conjugated π -ring system of the macrocycle or, in the case of $\text{TFcCorrFe}^{\text{III}}(\text{NO})$, at the NO axial ligand which can exist as a neutral NO, NO^+ or NO^- .³⁰⁻³² The assignments of the electron transfer site is sometimes straightforward but, in other cases, it is not as clear, due to the reported non-innocence of the corrole ligand, which, in the case of iron complexes, have been described as $[\text{Fe}^{\text{IV}}(\text{Corr}^{3-})]^{33}$ or $[\text{Fe}^{\text{III}}(\text{Corr}^{\bullet 2-})]^{34}$ by different research groups.

The cyclic voltammogram for $\text{TFcCorrFe}^{\text{IV}}(\text{Cl})$ is different than that of $\text{TFcCorrFe}^{\text{III}}(\text{NO})$ or $\text{TFcCorrFe}^{\text{IV}}(\text{C}_6\text{H}_5)$. The product of first irreversible reduction at -1.42 V is proposed to be the $[\text{TFcCorrFe}^{\text{III}}(\text{Cl})]^-$ anion. After the second reduction, the bound chloride ligand dissociates and the irreversible $\text{Fe}(\text{III})/\text{Fe}(\text{II})$ process at $E_{\text{pc}} = -1.42$ V is coupled to an $\text{Fe}(\text{II})/\text{Fe}(\text{III})$ reoxidation at $E_{\text{pa}} = -0.58$ V for a scan rate of 0.1 V/s.

Similar redox behavior has been reported for other Fe(IV) corroles³⁵⁻³⁸ and the proposed mechanism, based on data in the literature for related compounds, is given in Scheme 6-1.

The data on the iron corroles described in this chapter should be compared with earlier results for the same series of compounds when the measurements were carried out in PhCN containing 0.1 M TBAP as supporting electrolyte (see CVs in Figure 6-2). When using TBAP as supporting electrolyte, the oxidation of TFCorrFe^{III}(NO) involved a global three electron oxidation of the three Fc groups at the same potential of 0.61 V and the oxidation peak current of 9 μ A was three times that of the one electron reduction steps (3 μ A).³⁹ The two Fe(IV) corroles also undergo a global three electron oxidation of the Fc groups at 0.50 to 0.77 V.

As seen in Figure 6-1, the cyclic voltammograms of TFCorrFe^{III}(NO) and TFCorrFe^{IV}(C₆H₅) are characterized by reversible one-electron reductions at almost identical potentials of $E_{1/2} = -0.43$ and -1.83 V (for the iron-nitrosyl corrole) and $E_{1/2} = -0.43$ and -1.76 V (for the iron-phenyl derivative). Despite the similar reduction potentials, the prevailing redox processes in the first one-electron addition are quite different, formally Fe(IV)/(III) for the first reduction of TFCorrFe^{IV}(C₆H₅) and Fe(III)/(II) for the first reduction of TFCorrFe^{III}(NO). The basis of these assignments is given in part by comparison with data in the literature for other iron corroles containing phenyl and nitrosyl axial ligands.^{36,40,41}

The potentials for oxidation of the three ferrocene groups on the TFCorrFe derivatives are close to each other and completely overlapped in the case of

TFcCorrFe^{III}(NO) ($E_{1/2} = 0.61$ V), where the oxidation peak current of 9 μ A is three times that of the one-electron reduction steps (3 μ A). The fact that a single oxidation process is observed for the global three electron conversion of TFcCorrFe(NO) to [TFcCorrFe(NO)]³⁺ is consistent with the lack of communication between the three *meso*-Fc groups in their neutral or electrogenerated Fc⁺ forms.

Compared with Figure 6-1, TFcCorrFe^{IV}(C₆H₅) in solutions of TBAP is characterized by two reversible oxidations at 0.50 and 0.60 V while TFcCorrFe^{IV}(Cl) exhibits two reversible oxidation at $E_{1/2} = 0.61$ and 0.77 V. This means that changing the supporting electrolyte from TBAP to TFAB leads to a separation of the oxidation potentials for the three Fc substituents. The lower ion-pairing interaction of the [B(C₆F₅)₄]⁻ anion⁴² with the singly oxidized ferrocenyl groups leads to a larger separation of the oxidation waves.

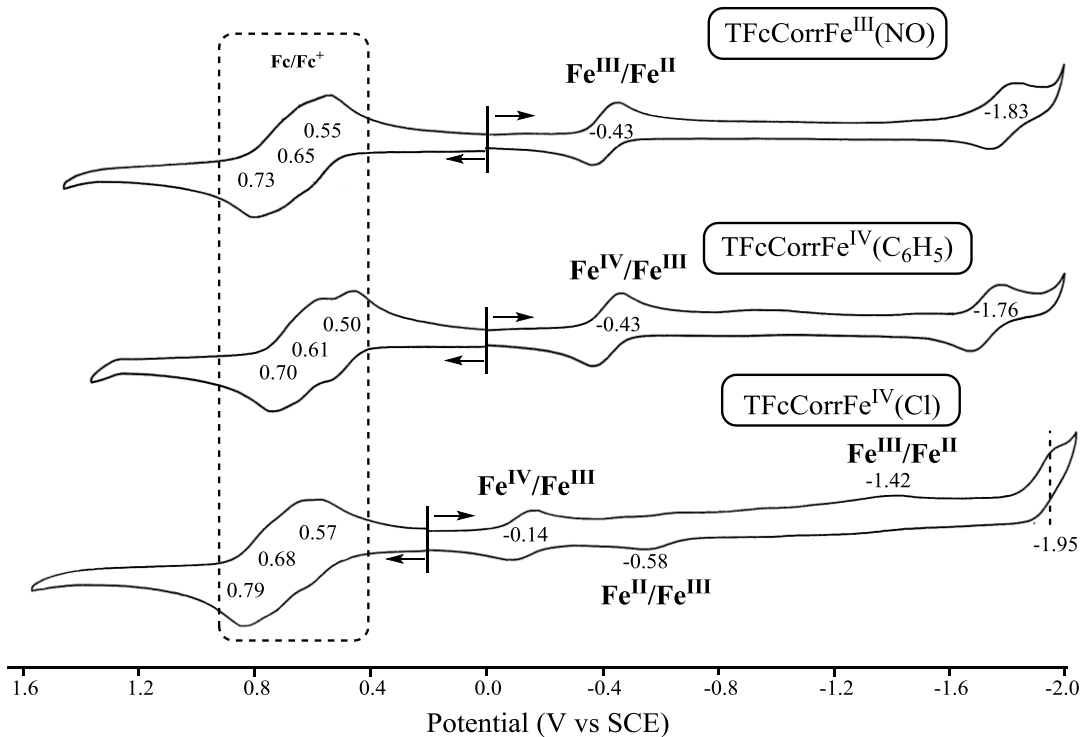


Figure 6-1. Cyclic voltammograms of TFcCorrFe^{III}(NO), TFcCorrFe^{IV}(C₆H₅) and TFcCorrFe^{IV}(Cl) in PhCN, containing 0.05 M TFAB at a scan rate of 0.1V/s.

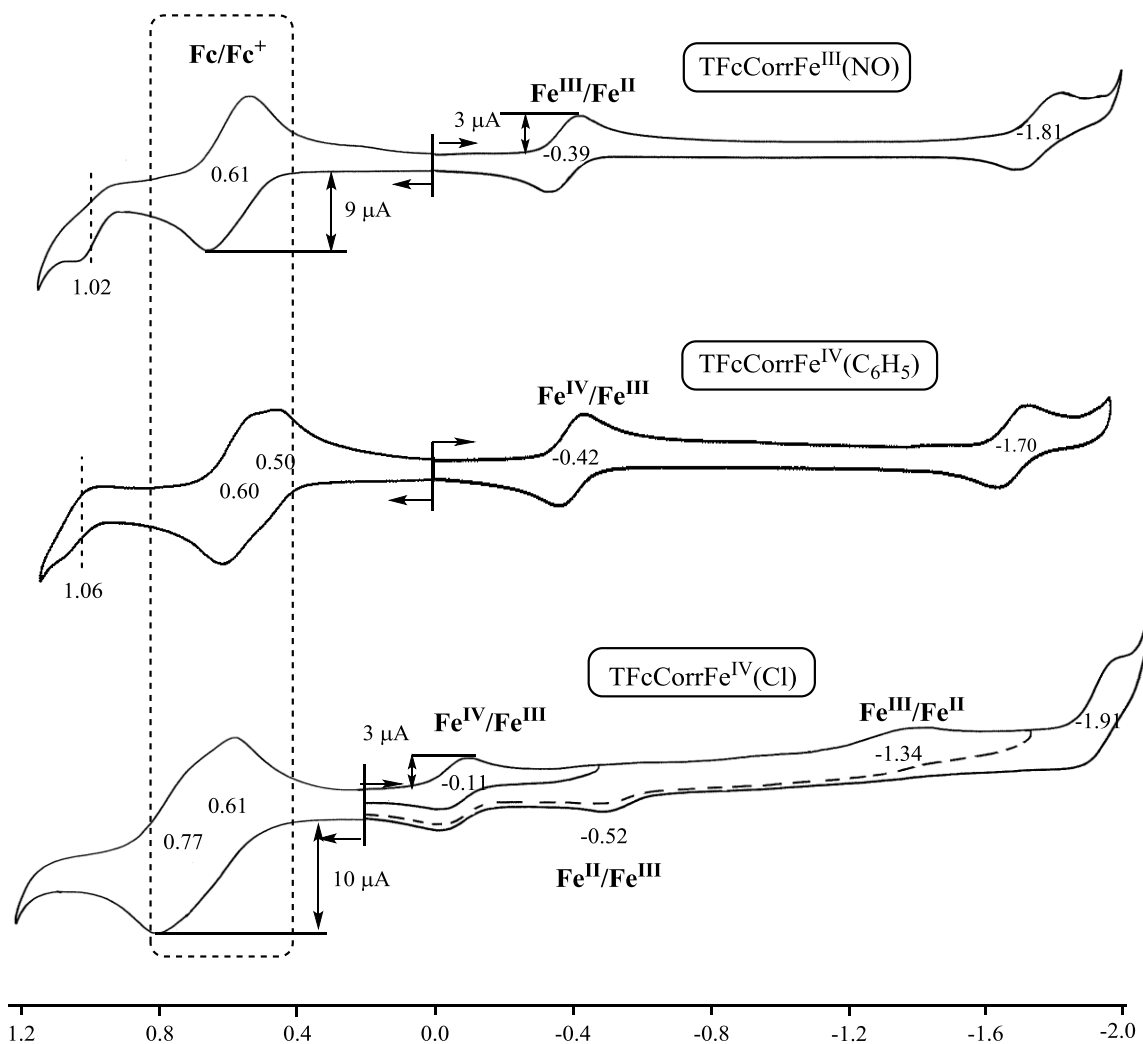
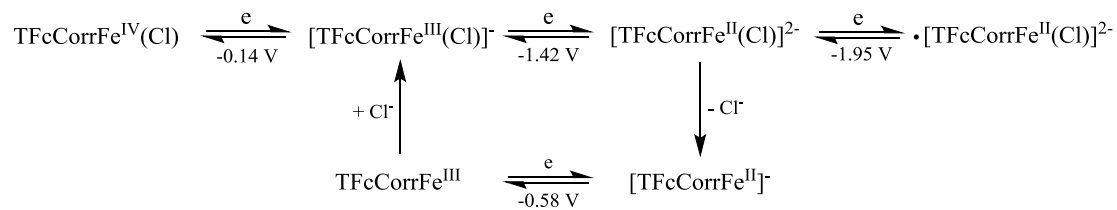


Figure 6-2. Cyclic voltammograms of TFCorrFe^{III}(NO), TFCorrFe^{III}(C₆H₅) and TFCorrFe^{IV}(Cl) in PhCN, containing 0.1 M TBAP at a scan rate of 0.1 V/s.



Scheme 6-1. Reduction mechanism of $\text{TFcCorrFe}^{\text{IV}}(\text{Cl})$ in PhCN, containing 0.05 M TFAB.

6.3 Conclusions

In this chapter we have reported the electrochemical characterization of iron ferrocenecorroles with different axial ligands in PhCN, containing 0.05 M TFAB. Under the given experimental conditions, both TFCorrFe^{III}(NO) and TFCorrFe^{IV}(C₆H₅) undergo two reductions while three reductions are seen for TFCorrFe^{IV}(Cl). Noteworthy is a comparison of the data with TFAB as supporting electrolyte and that which is observed for the same corroles, using 0.1 M TBAP as supporting electrolyte. Utilizing 0.05 M TFAB as electrolyte can clearly separate the three reversible oxidations of the Fc substituents.

6.4 References

- (1) Nemykin, V. N.; Rohde, G. T.; Barrett, C. D.; Hadt, R. G.; Sabin, J. R.; Reina, G.; Galloni, P.; Floris, B. *Inorganic Chemistry* **2010**, *49*, 7497.
- (2) Shoji, O.; Okada, S.; Satake, A.; Kobuke, Y. *J. Am. Chem. Soc.* **2005**, *127*, 2201.
- (3) Shoji, O.; Tanaka, H.; Kawai, T.; Kobuke, Y. *J. Am. Chem. Soc.* **2005**, *127*, 8598.
- (4) Nemykin, V. N.; Rohde, G. T.; Barrett, C. D.; Hadt, R. G.; Bizzarri, C.; Galloni, P.; Floris, B.; Nowik, I.; Herber, R. H.; Marrani, A. G.; Zanoni, R.; Loim, N. M. *J. Am. Chem. Soc.* **2009**, *131*, 14969.
- (5) Kubo, M.; Mori, Y.; Otani, M.; Murakami, M.; Ishibashi, Y.; Yasuda, M.; Hosomizu, K.; Miyasaka, H.; Imahori, H.; Nakashima, S. *The Journal of Physical Chemistry A* **2007**, *111*, 5136.
- (6) Hitchcock, P. B.; McLaughlin, G. M. *J. Chem. Soc., Dalton Trans.* **1976**, 1927.
- (7) Rohde, G. T.; Sabin, J. R.; Barrett, C. D.; Nemykin, V. N. *New Journal of Chemistry* **2011**, *35*, 1440.
- (8) Nemykin, V. N.; Barrett, C. D.; Hadt, R. G.; Subbotin, R. I.; Maximov, A. Y.; Polshin, E. V.; Kuposov, A. Y. *Dalton Transactions* **2007**, 3378.
- (9) Bucher, C.; Devillers, C. H.; Moutet, J.-C.; Royal, G.; Saint-Aman, E. *Coordination Chemistry Reviews* **2009**, *253*, 21.
- (10) Solntsev, P. V.; Neisen, B. D.; Sabin, J. R.; Gerasimchuk, N. N.; Nemykin, V. N. *Journal of Porphyrins and Phthalocyanines* **2011**, *15*, 612.
- (11) Nemykin, V. N.; Kobayashi, N. *Chem. Commun. (Cambridge)* **2001**, 165.
- (12) Lukyanets, E. A.; Nemykin, V. N. *Journal of Porphyrins and Phthalocyanines* **2010**, *14*, 1.
- (13) Lukyanets, E. A.; Nemykin, V. N. *J. Porphyrins Phthalocyanines* **2010**, *14*, 1.
- (14) González-Cabello, A.; Vázquez, P.; Torres, T. *Journal of Organometallic Chemistry* **2001**, *637–639*, 751.
- (15) González-Cabello, A.; Claessens, C. G.; Martin-Fuch, G.; Ledoux-Rack, I.; Vázquez, P.; Zyss, J.; Agulló-López, F.; Torres, T. *Synthetic Metals* **2003**, *137*, 1487.
- (16) Pomarico, G.; Vecchi, A.; Mandoj, F.; Bortolini, O.; Cicero, D. O.; Galloni, P.; Paolesse, R. *Chem. Commun. (Cambridge, U. K.)* **2014**, *50*, 4076.
- (17) Kumar, R.; Misra, R.; PrabhuRaja, V.; Chandrashekar, T. K. *Chem. - Eur. J.* **2005**, *11*, 5695.
- (18) Venkatraman, S.; Kumar, R.; Sankar, J.; Chandrashekar, T. K.; Sendhil, K.; Vijayan, C.; Kelling, A.; Senge, M. O. *Chem. - Eur. J.* **2004**, *10*, 1423.
- (19) Gryko, D. T.; Piechowska, J.; Jaworski, J. S.; Galezowski, M.; Tasiór, M.; Cembor, M.; Butenschon, H. *New Journal of Chemistry* **2007**, *31*, 1613.
- (20) Gust, D.; Moore, T. A.; Moore, A. L. *Accounts of Chemical Research* **1993**, *26*, 198.
- (21) Wasielewski, M. R. *Chemical Reviews* **1992**, *92*, 435.

- (22) Heath, J. R.; Kuekes, P. J.; Snider, G. S.; Williams, R. S. *Science (Washington, D. C.)* **1998**, *280*, 1716.
- (23) Chen, Y.; Jung, G.-Y.; Ohlberg, D. A. A.; Li, X.; Stewart, D. R.; Jeppesen, J. O.; Nielsen, K. A.; Stoddart, J. F.; Williams, R. S. *Nanotechnology* **2003**, *14*, 462.
- (24) Beer, P. D.; Gale, P. A.; Chen, G. Z. *Coordination Chemistry Reviews* **1999**, *185–186*, 3.
- (25) Bard, A. J. *Nature (London)* **1995**, *374*, 13.
- (26) Matsushige, K.; Yamada, H.; Tada, H.; Horiuchi, T.; Chen, X. Q. *Ann. N. Y. Acad. Sci.* **1998**, *852*, 290.
- (27) Liu, Z.; Yasseri, A. A.; Lindsey, J. S.; Bocian, D. F. *Science (Washington, DC, U. S.)* **2003**, *302*, 1543.
- (28) Day, P.; Hush, N. S.; Clark, R. J. H. *Philos. Trans. R. Soc., A* **2008**, *366*, 5.
- (29) Hadt, R. G.; Nemykin, V. N. *Inorg. Chem.* **2009**, *48*, 3982.
- (30) Vazquez-Lima, H.; Norheim, H.-K.; Einrem, R. F.; Ghosh, A. *Dalton Trans.* **2015**, *44*, 10146.
- (31) Stefanelli, M.; Nardis, S.; Tortora, L.; Fronczek, F. R.; Smith, K. M.; Licoccia, S.; Paolesse, R. *Chem. Commun. (Cambridge, U. K.)* **2011**, *47*, 4255.
- (32) Sinha, W.; Deibel, N.; Agarwala, H.; Garai, A.; Schweinfurth, D.; Purohit, C. S.; Lahiri, G. K.; Sarkar, B.; Kar, S. *Inorg. Chem.* **2014**, *53*, 1417.
- (33) Simkhovich, L.; Goldberg, I.; Gross, Z. *Inorg. Chem.* **2002**, *41*, 5433.
- (34) Walker, F. A.; Licoccia, S.; Paolesse, R. *J. Inorg. Biochem.* **2006**, *100*, 810.
- (35) Richter-Addo, G. B.; Hodge, S. J.; Yi, G.-B.; Khan, M. A.; Ma, T.; Van Caemelbecke, E.; Guo, N.; Kadish, K. M. *Inorg. Chem.* **1996**, *35*, 6530.
- (36) Simkhovich, L.; Mahammed, A.; Goldberg, I.; Gross, Z. *Chem. - Eur. J.* **2001**, *7*, 1041.
- (37) Steene, E.; Wondimagegn, T.; Ghosh, A. *J. Phys. Chem. B* **2001**, *105*, 11406.
- (38) Steene, E.; Dey, A.; Ghosh, A. *J. Am. Chem. Soc.* **2003**, *125*, 16300.
- (39) Pomarico, G.; Galloni, P.; Mandoj, F.; Nardis, S.; Stefanelli, M.; Vecchi, A.; Lentini, S.; Cicero, D. O.; Cui, Y.; Zeng, L.; Kadish, K. M.; Paolesse, R. *Inorg. Chem.* **2015**, *54*, 10256.
- (40) Van Caemelbecke, E.; Will, S.; Autret, M.; Adamian, V. A.; Lex, J.; Gisselbrecht, J.-P.; Gross, M.; Vogel, E.; Kadish, K. M. *Inorg. Chem.* **1996**, *35*, 184.
- (41) Nardis, S.; Stefanelli, M.; Mohite, P.; Pomarico, G.; Tortora, L.; Manowong, M.; Chen, P.; Kadish, K. M.; Fronczek, F. R.; McCandless, G. T.; Smith, K. M.; Paolesse, R. *Inorg. Chem.* **2012**, *51*, 3910.
- (42) Camire, N.; Mueller-Westerhoff, U. T.; Geiger, W. E. *J. Organomet. Chem.* **2001**, *637-639*, 823.